The soil-borne white root rot pathogen *Rosellinia necatrix* expresses antimicrobial proteins during host colonization

Edgar A. Chavarro-Carrero[1,2], Nick C. Snelders[2,3,$], David E. Torres[1,3,$], Anton Kraege[2], Ana López-Moral[2], Gabriella C. Petti[2], Wilko Punt[2], Jan Wieneke[2], Rómulo García-Velasco[4], Carlos J. López-Herrera[5], Michael F. Seidl[3,#] and Bart P.H.J. Thomma[1,2,#,‡]

[1]Laboratory of Phytopathology, Wageningen University & Research, 6708 PB Wageningen, The Netherlands.

[2]Institute for Plant Sciences, Cluster of Excellence on Plant Sciences (CEPLAS), University of Cologne, Cologne, Germany

[3]Theoretical Biology & Bioinformatics Group, Department of Biology, Utrecht University, Utrecht, The Netherlands

[4]Laboratory of Phytopathology, Tenancingo University Center, Autonomous University of the State of Mexico, Tenancingo, State of Mexico, Mexico.

[5]CSIC, Instituto de Agricultura Sostenible, Dept. Protección de Cultivos, C/Alameda del Obispo s/n, 14004, Córdoba, Spain.

Short title: *Rosellinia necatrix* antimicrobial effector proteins

[$]These authors contributed equally

[#]These authors contributed equally

[‡]Corresponding author: B.P.H.J. Thomma; Telephone: 0049-221-47089261; E-mail: bthomma@uni-koeln.de

ABSTRACT

Rosellinia necatrix is a prevalent soil-borne plant-pathogenic fungus that is the causal agent of white root rot disease in a broad range of host plants. The limited availability of genomic resources for *R. necatrix* has complicated a thorough understanding of its infection biology. Here, we sequenced nine *R. necatrix* strains with Oxford Nanopore sequencing technology, and with DNA proximity ligation we generated a gapless assembly of one of the genomes into ten chromosomes. Whereas many filamentous pathogens display a so-called two-speed genome with more dynamic and more conserved compartments, the *R. necatrix* genome does not display such genome compartmentalization. It has recently been proposed that fungal plant pathogens may employ effectors with antimicrobial activity to manipulate the host microbiota to promote infection. In the predicted secretome of *R. necatrix*, 26 putative antimicrobial effector proteins were identified, nine of which are expressed during plant colonization. Two of the candidates were tested, both of which were found to possess selective antimicrobial activity. Intriguingly, some of the inhibited bacteria are antagonists of *R. necatrix* growth *in vitro* and can alleviate *R. necatrix* infection on cotton plants. Collectively, our data show that *R. necatrix* encodes antimicrobials that are expressed during host colonization and that may contribute to modulation of host-associated microbiota to stimulate disease development.

46 **INTRODUCTION**

47 *Rosellinia necatrix* is a prevalent soil-borne plant-pathogenic fungus that is found
48 in temperate and tropical areas worldwide (Sivanesan and Holliday, 1972). As
49 causal agent of white root rot disease, *R. necatrix* has a broad host range
50 comprising at least 170 species of dicotyledonous angiosperms that are
51 dispersed over 63 genera and 30 families (Sztejnberg and Madar, 1980). Many of
52 these species are of great economic importance, such as *Coffea* spp. (coffee),
53 *Malus* spp. (apple), *Olea europea* L. (olive), *Persea americana* Mill. (avocado),
54 *Prunus* spp. (peaches, almonds, etc.), *Vitis vinifera* L. (grape) (Eguchi et al.,
55 2009) and *Rosa* sp. (rose) (García-Velasco et al., 2012).

56 Plants infected by *R. necatrix* usually display two types of symptoms. The
57 first type is displayed below-ground on the root system, where white and black
58 colonies of mycelium can occur on the surface of infected roots. As the fungus
59 penetrates and colonizes the root tissue, the roots acquire a dark brown color
60 (Guillaumin et al., 1982). The second type of symptom occurs above-ground.
61 These symptoms can develop rapidly as a consequence of the damaged root
62 system and comprise wilting of leaves, typically after a period of drought or
63 physiological stress, which affects plant vigor and eventually can lead to plant
64 death. Symptoms of *R. necatrix* infection can also appear slowly, leading to a
65 decline in growth, decreasing leaf numbers, along with wilting of leaves,
66 chlorosis, and death of twigs and branches. On perennials these symptoms
67 aggravate over time, and when moisture and temperature are unfavorable, the
68 plant eventually dies (Guillaumin et al., 1982).

69 Various studies have addressed the biology of *R. necatrix* (Pérez-Jiménez
70 et al., 2002; Pliego et al., 2009). Nevertheless, the molecular mechanisms
71 underlying pathogenicity of *R. necatrix* remain largely unexplored, mainly

because the limited availability of genomic resources to date complicates investigations into the molecular biology of *R. necatrix* infections. Until recently, only a single Illumina technology short-read sequencing-based *R. necatrix* draft genome assembly was generated of strain W97 that was isolated from apple in Japan (Shimizu et al., 2018). This 44 Mb genome assembly is highly fragmented as it comprises 1,209 contigs with 12,444 predicted protein-coding genes (Shimizu et al., 2018). Recently, another assembly was released of a South-African strain (CMW50482) that was isolated from avocado, yet this assembly is even more fragmented with 1,362 contigs (Wingfield et al., 2022).

It is generally accepted that plant pathogens secrete dozens to hundreds of so-called effectors into their host plants to stimulate host colonization (Rovenich et al., 2014; Wilson and McDowell, 2022). Effectors can be defined as small, secreted proteins of ≤300 amino acids that are cysteine-rich and have tertiary structures that are stabilized by disulfide bridges and that are secreted by pathogens to promote disease on plant hosts (Duplessis et al., 2011; Gan et al., 2013; Stergiopoulos et al., 2013; Lo Presti et al., 2015). However, also larger secreted proteins have been found to act as effectors, such as several LysM effectors (Djamei et al., 2011; Kombrink and Thomma, 2013). Furthermore, also non-proteinaceous effectors have been described, such as fungal secondary metabolites as well as small RNA (sRNA) molecules that are delivered into host cells to suppress host immunity (Weiberg et al., 2014). Many effectors have been shown to act in suppression of host immune responses (Rovenich et al., 2014). However, recent studies have uncovered additional functions of pathogen effector proteins in host colonization (Wilson and McDowell, 2022). For example, the soil-borne pathogen *Verticillium dahliae* secretes effector proteins to modulate microbiota compositions inside the host

98 plant as well as outside the host in the soil to support host colonization (Snelders
99 et al., 2020; 2021; 2022; 2023). One of them is the effector protein VdAve1 that
100 was shown to display selective antimicrobial activity and facilitate colonization of
101 tomato and cotton plants through host microbiota manipulation by suppressing
102 antagonistic bacteria, such as members of the *Spingomonadaceae* (Snelders et
103 al., 2020). Besides VdAve1, ten additional potentially antimicrobial effector
104 protein candidates were predicted by mining the *V. dahliae* secretome for
105 structural homologues of known antimicrobial proteins (AMPs) (Snelders et al.,
106 2020). One of these candidates, VdAMP2, was subsequently found to contribute
107 to *V. dahliae* survival in soil through its efficacy in microbial competition
108 (Snelders et al., 2020). Another candidate, VdAMP3, was shown to promote
109 microsclerotia formation in decaying host tissue through its antifungal activity
110 directed against fungal niche competitors (Snelders et al., 2021). Most recently,
111 a multiallelic gene homologous to *VdAve1* was identified as *VdAve1-like*
112 (*VdAve1L*) of which the *VdAve1L2* variant was shown to encode an effector that
113 promotes tomato colonization through suppression of antagonistic Actinobacteria
114 in the host microbiota (Snelders et al., 2023). These findings have led to the
115 hypothesis that microbiota manipulation is a general virulence strategy of plant
116 pathogens to promote host colonization (Snelders et al., 2022). However, thus
117 far evidence for such activity has been lacking for other fungal plant pathogens.

118 Similar to *V. dahliae*, also *R. necatrix* is a soil-borne pathogen that spends
119 at least part of its life cycle in the soil, known to be an extremely competitive
120 and microbe-rich environment (Smercina et al., 2021). In the present study, we
121 aimed to generate a high-quality genome assembly to mine the *R. necatrix*
122 genome for potential antimicrobial proteins that are exploited during host
123 colonization and test the hypothesis that other pathogenic fungi besides *V.*

124 *dahliae* exploit effector proteins with antimicrobial activity during host
125 colonization as well.

126 **RESULTS**

127 **A chromosome-level assembly of *Rosellinia necatrix* strain R18**

128 Thus far, two fragmented *R. necatrix* draft genome assemblies that comprise
129 over 1,200 contigs are publicly available (Shimizu et al., 2018; Wingfield et al.,
130 2022). To generate additional and more contiguous *R. necatrix* genome
131 assemblies, we sequenced nine strains of *R. necatrix* that were collected from
132 rose and avocado in Mexico and Spain, respectively, with Oxford Nanopore
133 sequencing technology (ONT). This resulted in genome assemblies of 28 (for
134 strain R18) to 399 (for strain CH12) contigs (Table 1). The most contiguous
135 assembly was obtained for strain R18, isolated from infected rose plants in
136 Mexico.

137 **Table 1. Sequencing summary and genome assembly statistics for nine *Rosellinia necatrix* strains.**

Strain name	**Rn19[a]**	**CH12[a]**	**Rn400[a]**	**R10[a]**	**R25[a]**	**R27[a]**	**R28[a]**	**R30[a]**	**R18[a]**	**R18[b]**
Isolated from	Avocado	Avocado	Avocado	Rose	Rose	Rose	Rose	Rose	Rose	
Country of origin	Spain	Granada, Spain	Granada, Spain	State of Mexico, Mexico	State of Mexico, Mexico	State of Mexico, Mexico	State of Mexico, Mexico	State of Mexico, Mexico	State of Mexico, Mexico	
Year	2001	1988	1991	2005	2008	2005	2011	2014	2014	
Read N50 (kb)	23	17	21	18	16	21	21	9	18	**30**
Coverage	45X	46X	35X	35X	45X	46X	41X	52X	42X	**120X**
No. of contigs	35	399	37	50	58	31	47	130	28	**11**
Total length (Mb)	48.2	49.9	48.2	48.9	49.2	49.2	48.7	48.3	49	**49.1**
Average length (Mb)	1.3	0.1	1.3	1	0.8	1.5	1	0.3	0.8	**4**
Maximum length (Mb)	6.4	6.3	5.8	4.4	4	6.4	6.4	4.5	4	**7.1**
N50 (Mb)	3.4	4.6	3.8	1.9	2.5	3.2	3.4	1.6	3.1	**5.1**
N90 (Mb)	0.8	3.1	1.3	0.4	0.5	1.2	0.8	0.3	0.6	**3.3**
GC (%)	46.28	46.37	46.37	45.35	45.49	45.43	45.50	45.99	45.35	**45.46**
BUSCO (%)	76.7	69.9	70.2	68.4	78.9	72.3	68.2	80.7	82.5	**97**

138 [a]*de novo* assembly based on Nanopore sequencing of high-molecular weight (HMW) DNA.

139 [b]*de novo* assembly based on Nanopore sequencing of HMW and UHMW DNA and Hi-C sequencing.

140 To further improve the genome assembly of strain R18, additional ONT
141 sequencing was performed using ultra HMW (UHMW) DNA as template.
142 Additionally, chromosome conformation capture (Hi-C) followed by high-
143 throughput sequencing was performed (Burton et al., 2013; Varoquaux et al.,
144 2015). Based on these orthogonal sequencing data, we ultimately assembled the
145 R18 genome into 11 contigs (Table 1). Using Tapestry (Davey et al., 2020)
146 twenty telomeric regions ([TTAGGG]*n*) were identified (Fig. 1A), and ten of the
147 11 contigs were found to contain telomeric regions at both ends, suggesting that
148 these represent completely assembled chromosomes, which could be confirmed
149 by Hi-C analysis (Fig. 1B). The 11th, and smallest, contig contained no telomeric
150 regions, displayed a markedly higher coverage (read depth) (Fig. 1B), and BLAST
151 analysis revealed hits to fungal mitochondrial genomes, showing that this contig
152 belongs to the mitochondrial genome. Accordingly, no mitochondrial genes could
153 be found on any of the ten chromosomal contigs. Thus, we conclude that our
154 assembly contains ten complete chromosomes that compose the nuclear
155 genome, and an 11th contig that composes the mitochondrial genome, and thus
156 that we generated a gapless, telomere-to-telomere, genome assembly. To
157 measure the completeness of the genome assembly, we used BUSCO v4 with the
158 Ascomycota dataset (Simão et al., 2015), which resulted in a completeness score
159 of 97%.

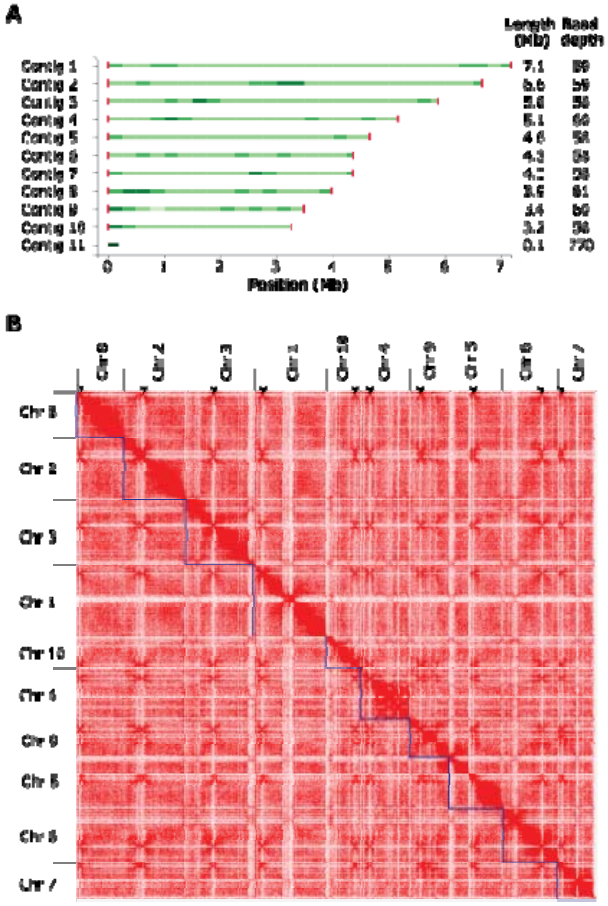

Figure 1. Genome assembly of *Rosellinia necatrix* strain R18. (A) Genome assembly plot generated with Tapestry (Davey et al., 2020). Green bars indicate contig sizes with the color intensity correlating with read coverage, while red bars indicate telomeres with the color intensity correlating with the number of telomeric repeats. Contig 11 lacks telomeres and represents the mitochondrial genome. (B) Hi-C contact matrix showing interaction frequencies between regions in the genome of *Rosellinia necatrix* strain R18. Ten regions with high inter-chromosomal interaction frequencies are indicative of centromeres and are indicated with arrowheads.

To further explore the *R. necatrix* strain R18 assembly, genome annotation was performed using Funannotate (Palmer and Stajich, 2017) guided by publicly available RNAseq data (Shimizu et al., 2018), resulting in 11,760 predicted protein-coding genes (Table 2). Furthermore, effector genes were predicted using EffectorP (Sperschneider et al., 2018). The assembled genome of *R. necatrix* strain R18 was predicted to encode 1,126 secreted proteins, of which 192 were predicted to be effector candidates. BLAST searches revealed that 182

177 of these have homology to Ascomycete fungal proteins, of which 69 had
178 functional domain annotations, while the remaining 113 were annotated as
179 hypothetical proteins (Supplemental Table 1). The largest group of annotated
180 effectors were cell wall degrading enzymes, including glycoside hydrolases and
181 carbohydrate esterases that are generally involved in plant cell wall degradation
182 (Underwood, 2012; Malinovsky et al., 2014). Effectors carrying carbohydrate-
183 binding domains while lacking enzymatic domains, specifically a concanavalin A-
184 like lectin and two cell wall integrity and stress response component (WSC)
185 domain-containing proteins, were also found. Concanavalin A-like lectin has been
186 described as a virulence factor, although no molecular mechanism has been
187 presented (Ismail and Able, 2016), while WSC domain-containing proteins can
188 protect fungal cell wall through structural strengthening, but their contribution to
189 plant colonization remains unclear (Wawra et al., 2019). Additionally, two lysin
190 motif (LysM) effectors were found that typically bind chitin and play roles in
191 virulence through suppression of chitin-triggered immunity or shielding hyphae
192 against host-derived chitinases (de Jonge et al., 2010; Kombrink and Thomma,
193 2013; Tian et al., 2021; 2022). Four genes were found to encode hydrophobins;
194 proteins that have been implicated in virulence through acting as phytotoxin
195 (Takai, 1974), or promoting attachment to plant surfaces and appressoria
196 formation (Talbot et al., 1996), although negative impacts on host colonization
197 have also been reported (Luciano-Rosario et al., 2022). Finally, three potential
198 toxins were found, namely a cerato-platanin domain-containing protein (Carresi
199 et al., 2006) and two necrosis and ethylene-inducing-like (NLP) effectors that are
200 typically thought to be phytotoxic to eudicot plants (Lenarčič et al., 2017; Seidl &
201 van den Ackerveken, 2019) (Supplemental Table 1).

202 To investigate the conservation of effector gene catalogues among the *R.*
203 *necatrix* genomes that we sequenced in our study, we performed BLAST searches
204 to find homologs of each of the predicted effector genes in the genome of strain
205 R18 in each of the other genomes. Intriguingly, we found remarkably little
206 presence-absence variation, with only few effector genes missing in some of the
207 other genomes. While strains R27, R28 and R30 carry all the effector genes that
208 were identified in strain R18, strain R10 and R25 lack two, strains R19 lacks
209 three, and strains CH12 and Rn400 lack four of the 192 predicted effector genes
210 (Supplemental Table 2). Furthermore, we determined the ratio of single
211 nucleotide polymorphisms (SNPs) for each of the predicted effectors.
212 Interestingly, while strains Rn19 and strain Rn400 share no identical effector
213 genes and strain CH12 only a single identical effector gene with strain R18, on
214 the other end of the spectrum strain R10 shares 152 identical effector genes with
215 strain R18. Furthermore, SNP ratios vary from 0% up to 26,12% for effector
216 *FUN_011522* in strain CH12. Generally, we observed higher variability in
217 effectors of the Spanish strains (Rn19, CH12, Rn400) than in the Mexican strains
218 (R10, R25, R27, R28, R30) (Supplemental Table 2).
219

220 **Table 2. Genome annotation of *Rosellinia necatrix* strain R18.**

Genomic trait	Value
Protein-coding genes (Funannotate version 1.8.13, Palmer and Stajich, 2017)	11,760
Mean gene length (bp)	1,689.48
Mean exons per gene	2.92
Mean intergenic length (bp)	1,114
Homologs in InterPro database	8,125
Secreted proteins (SignalP; version 5.0, Almagro et al., 2019)	1,126
Effectors (EffectorP; version 2.0, Sperschneider et al., 2018)	192
CAZymes (Funannotate)	535
CAZymes (secreted) (Funannotate)	300

Small cysteine-rich proteins (Funannotate)	209
LysM (lysin motif) effectors (Funannotate)	2
NLP (necrosis and ethylene-inducing-like) effectors (Funannotate)	2
Secondary metabolite clusters (antiSMASH; version 5.0, Blin et al., 2019)	48

Besides proteinaceous effectors, 48 secondary metabolite gene clusters were predicted using antiSMASH fungal version (Blin et al., 2019; Table 2). From these, 13 showed homology to known secondary metabolite clusters, including those for the production of swainsonine, cytochalasin E/K, pyriculol, enniatin, and naphthalene, which have been implicated in pathogenicity through their phytotoxic activity (Thomas, 1978; Sawai et al., 1983; Walton, 1990; Shimizu et al., 2014; Cook et al., 2017; Zhao et al., 2019; Xu et al., 2021), and copalyl diphosphate which has been implicated in elongation disorders in plants (Rademacher and Graebe, 1979; Kawaide, 2006) (Supplemental Table 3).

Absence of distinctive genome compartmentalization

In many filamentous pathogens, effector genes are found in repeat-rich and gene sparse genomic compartments, whereas they are depleted in repeat-poor and gene-dense regions that typically harbor housekeeping genes, a genome organization that is typically referred to as the two-speed genome (Frantzeskakis et al., 2020). Thus, we aimed to explore if effector genes were associated with repetitive regions in *R. necatrix* too. Interestingly, the repeat content in *R. necatrix* strain R18 is low (2.39%) and evenly distributed throughout the genome, with the most abundant families being DNA/Helitron (67%) and long terminal repeats (LTRs; 31%). Accordingly, most repetitive elements are not preferentially located near effectors ($p>0.05$ after permutation test for distance). Moreover, effector genes are not preferentially found in regions with large

244 intergenic distances (Fig. 2). Thus, our results do not support association of

245 effector genes with repeat-rich regions in *R. necatrix*.

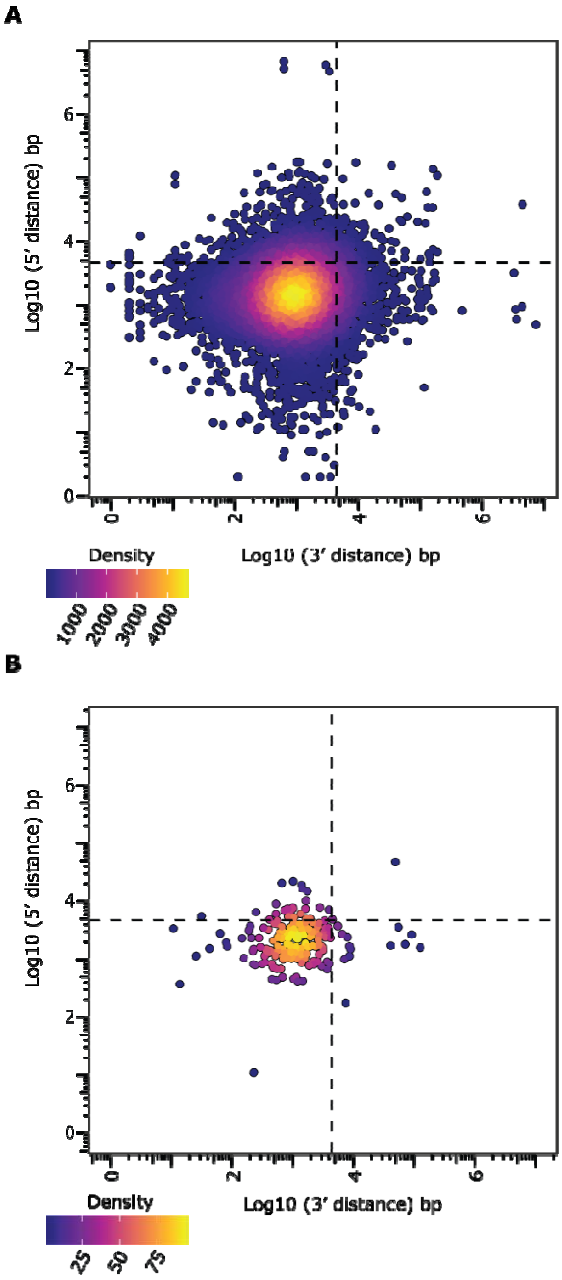

246

247 **Figure 2**. **Effector genes do not localize in gene-sparse regions.** Gene density

248 plot of '5 and '3 flanking log10 transformed intergenic distance with the dashed lines

249 depicting the mean intergenic distances for all genes (A) and candidate effector

250 genes encoded in the *R. necatrix* genome (B).

251

252 Genomic comparisons in various filamentous fungi have revealed extensive
253 chromosomal rearrangements and structural variants (SVs) in close association
254 with effector genes (Torres et al., 2020; Faino et al., 2016; Oggenfuss et al.,
255 2021; Fouché et al., 2020; Shi-Kunne et al., 2018). Thus, we tested whether
256 effector genes are associated with SVs in *R. necatrix*. First, to explore the
257 genomic diversity among *R. necatrix* strains, a phylogenetic tree of all genomes
258 was constructed with Realphy (version 1.12) (Bertels *et al.,* 2014). Two clusters
259 were identified, one with strains from Mexico isolated from roses, and one cluster
260 with the strains from Spain and South Africa, isolated from avocado, as well as
261 Japan, isolated from apple (Fig. 3). Then, SVs were predicted for each of the
262 genomes sequenced in this study using NanoSV (version 1.2.4 with default
263 settings; Stancu et al., 2017) by identifying split- and gapped-aligned long reads
264 for the various strains to define breakpoint-junctions of structural variations
265 when using the gapless genome assembly of strain R18 as a reference. We
266 retrieved 2,639 SVs in total, comprising 1,264 insertions, 1,344 deletions, 4
267 inversions and 27 translocations (Fig. 3A). The number of SVs per strain
268 corresponds to their phylogenetic relationships based on whole-genome
269 comparisons. To investigate the occurrence of the SVs in the *R. necatrix* strains,
270 we calculated the frequency of each SV over the strains used in the analysis.
271 Most of the SVs (94.2%) are shared by <50% of the strains, meaning that they
272 occur in less than four strains. This suggests that SV is a common phenomenon
273 in line with the phylogenetic and geographic relationship of *R. necatrix* strains.
274 Interestingly, SVs occur all across the genome (Fig. 3B), largely independently of
275 repetitive regions ($p>0.05$ after permutation test for distance), but are found in
276 close association with effector genes ($p<0.05$ after permutation test for
277 distance). Collectively, our results for *R. necatrix* substantiate the lack of the

typical genome compartmentalization that is associated with the two-speed genome organization that was found in many other filamentous fungi (Raffaele and Kamoun, 2012).

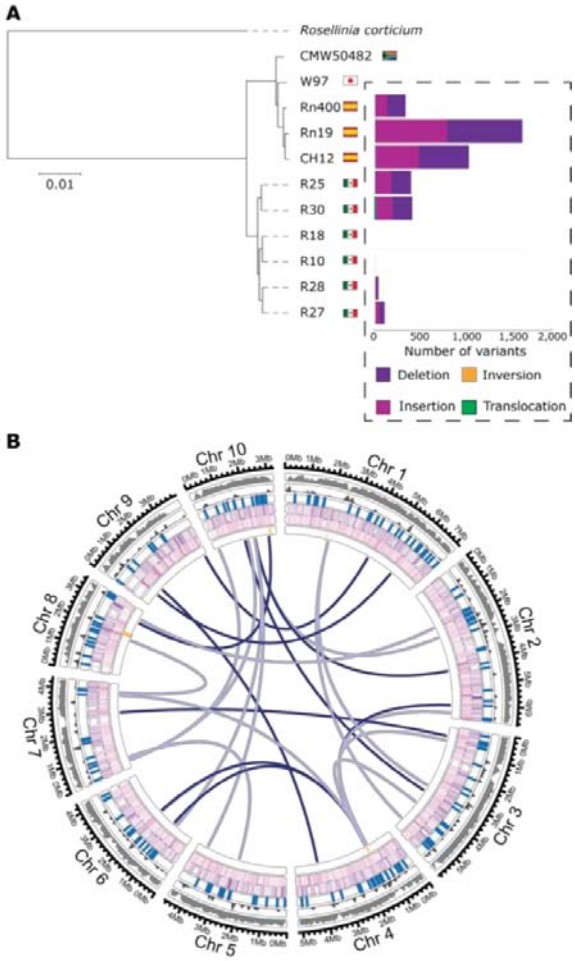

Figure 3. **Phylogeny and structural variation of nine *Rosellinia necatrix* strains.** (A) Phylogeny of sequenced *R. necatrix* strains was inferred using Realphy (Langmead and Salzberg, 2012). The robustness of the phylogeny was assessed using 1000 bootstrap replicates, and branch lengths represent sequence divergence. *Rosellinia corticium* was used to root the tree. The amount of structural variants was calculated using NanoSV (Stancu et al., 2017) using strain R18 as a reference. (B) Circular plot displaying the genomic distribution of 2,019 SVs along the 10 chromosomes of *R. necatrix*. The tracks are shown in the following order from outside to inside: Gene density (10 kb), repetitive density (10 kb), effector gene locations, deletions, insertions and inversions and translocations. The color intensity of the lines for each SV track depict frequency in the *R. necatrix* collection.

294 **Weak structural clustering in the effector catalog**

295 Effectors continuously evolve towards optimal functionality while simultaneously
296 evading recognition by plant immune receptors, which is considered one of the
297 reasons for the lack of sequence conservation among effector proteins. Despite
298 this lack of sequence conservation, groups of effector proteins that share their
299 three-dimensional structure have been identified in various filamentous
300 phytopathogens, such as the MAX-effector (*Magnaporthe* Avrs and ToxB like)
301 family of the rice blast fungus *Magnaporthe oryzae* (de Guillen et al., 2015) that,
302 together with some other families, are also found in the scab fungus *Venturia*
303 *inaequalis* (Rocafort et al., 2022). It has been speculated that MAX effectors
304 exhibit this structural conservation as an adaptation either to the apoplastic
305 environment, or for transport into the plant cytosol (de Guillen et al., 2015). To
306 investigate whether subsets of *R. necatrix* effectors display a similar fold
307 conservation, their structures were predicted with Alphafold2 with an average
308 quality score in a so-called predicted local distance difference test (pLDDT) of
309 86.1 (SD 11.8) on a scale from 0 to 100, with 100 indicating a perfect prediction.
310 As only 11% of the predicted structures scored lower than 70 and only 2% lower
311 than 50, we conclude that the fold prediction of the *R. necatrix* effector catalogue
312 is generally robust. Next, we performed similarity clustering of the predicted
313 effector folds, revealing that almost 40% of the effector candidates are
314 structurally unique, while the remaining effectors could be assigned to a total of
315 31 clusters. As these clusters were only small, with on average only four
316 members, we conclude that relatively little clustering occurs among *R. necatrix*
317 effectors.

318 To examine whether the observed clustering is merely based on structural
319 similarity, or is mainly driven by sequence conservation, the five largest clusters

320 that contain six to 11 members were further analysed (Fig. 4B, 4C). Two of the
321 five clusters show high average template modelling (TM) scores, with 0.85 and
322 0.91, respectively, on a scale from 0-1, while also showing a relatively high
323 degree of sequence conservation of 43 and 47 percent, respectively. The other
324 three clusters exhibit lower sequence conservation, with maximum 21 percent,
325 but also show considerably lower respectively structural conservation, with TM
326 scores between 0.57 and 0.64 only, indicating that structural similarity within the
327 clusters is positively correlating with sequence conservation. Hence, the
328 structural clustering can be explained by the sequence conservation amongst the
329 effector proteins. Taken together, although a considerable number of structural
330 effector clusters can be observed in *R. necatrix*, they contain only few members
331 and structural conservation is mostly based on sequence conservation. Thus,
332 effector family expansion seems to have played only a minor role in *R. necatrix*
333 effector evolution.

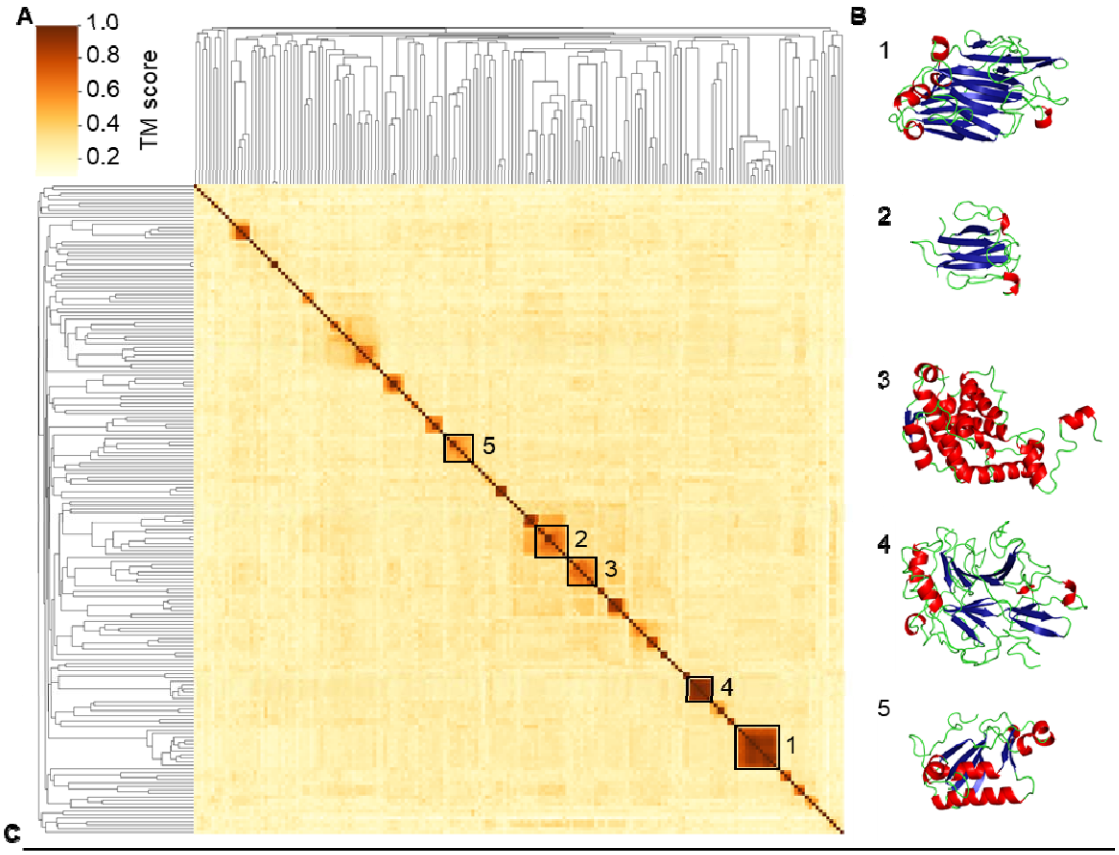

Cluster	Effector proteins	Average TM-score	Average Sequence identity	Annotation
1	11	0,85	43,47 %	Dehydrogenases
2	8	0,63	17,46 %	Glycoside hydrolases
3	7	0,64	21,27 %	Small secreted proteins
4	6	0,91	46,71 %	Cyanamide hydratases
5	6	0,57	18,29 %	Glucanosyl-transferases

Figure 4. *R. necatrix* effector candidates show weak structural clustering, which is based on sequence conservation. (A) Ordered by hierarchical clustering based on structural similarity, the heatmap displays the structural similarity of each effector pair in an all-vs-all alignment based on template modelling (TM) scores that range from 0 to 1. Effector clusters were identified based on a similarity threshold > 0.5. The five largest clusters are highlighted with a black square and ordered by size. (B) Example structure for each of the five clusters based on the effector with the highest similarity to other effectors in the cluster. (C) Characteristics of the five largest structural effector clusters.

Antimicrobial activity in culture filtrates

It has recently been proposed that fungal plant pathogens employ effectors with antimicrobial activity to manipulate the host microbiota to promote infection

348 (Rovenich et al., 2014; Wilson and McDowell, 2022; Snelders et al., 2022). To
349 explore if the soil-borne fungus *R. necatrix* potentially exploits antimicrobials, we
350 first tested whether *R. necatrix* culture filtrates can inhibit the growth of plant-
351 associated bacteria. To this end, we collected *R. necatrix* culture medium after 4,
352 7 and 9 days of fungal growth by filtration through a 0.45 nm filter, and an
353 aliquot of each of the culture filtrates was heat-inactivated at 95°C for 10
354 minutes. Finally, the culture filtrates were used as growth medium for individual
355 bacterial species from a diversity panel of 37 plant-associated bacteria
356 (Supplemental Table 4). After overnight incubation, growth of four of the 37
357 bacteria was inhibited in the 4- and 7-day culture medium filtrates when
358 compared with cultivation in the heat-inactivated culture filtrates, namely
359 *Bacillus drentensis, Achromobacter denitrificans, Sphingobium mellinum* and
360 *Flavobacterium hauense.* While three of these were not found to be inhibited
361 anymore in the 9-day culture medium filtrate, growth of *B. drentensis* was also
362 still inhibited in this filtrate (Fig. 5). Given that the heat-treatment inactivated
363 the antimicrobial activity, suggesting that the activity is of proteinaceous nature,
364 we passed the culture filtrates through a spin column with 3 kDa cut-off and
365 tested the growth of *Bacillus drentensis* and *Flavobacterium hauense* in these
366 filtrates. Interestingly, none of the filtrates inhibited bacterial growth, suggesting
367 that the activity is mediated by proteins that are retained in the spin column, as
368 metabolites and other small molecules are expected to pass through.
369 Collectively, these findings suggest that the culture medium of *R. necatrix*
370 contains (a) heat-sensitive protein(s) with selective antimicrobial activity.

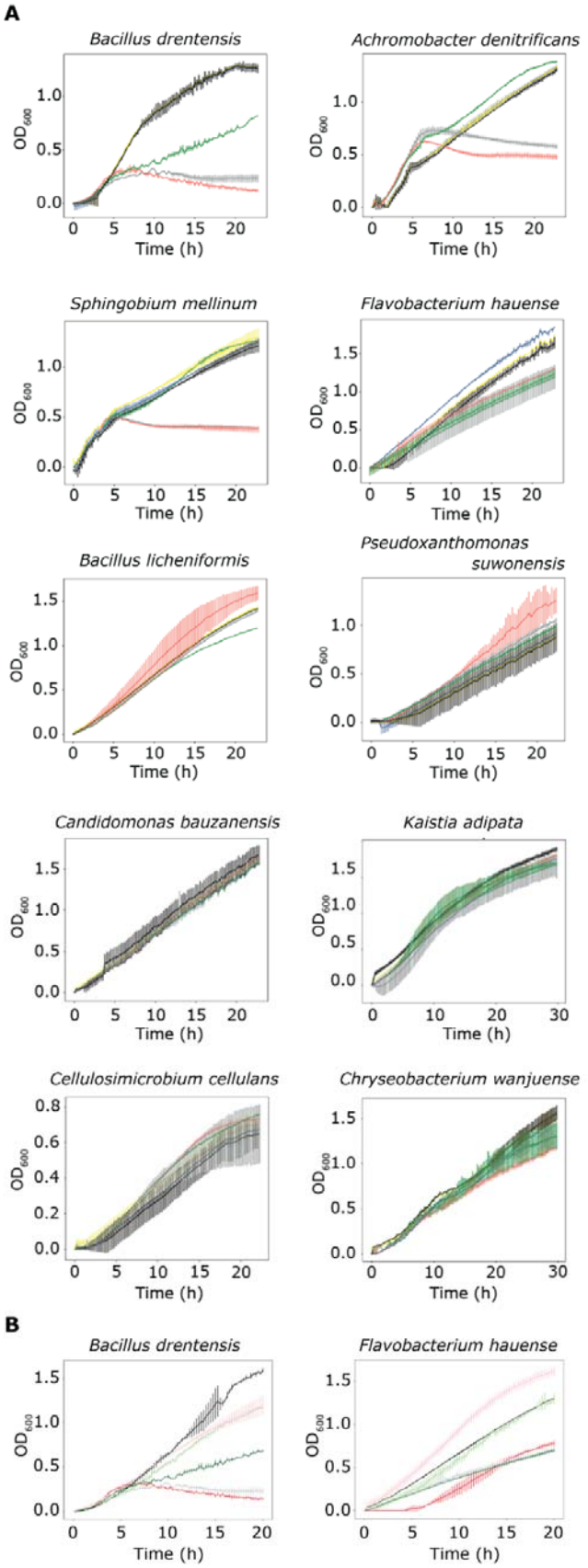
A
Bacillus drentensis
Achromobacter denitrificans
Sphingobium mellinum
Flavobacterium hauense
Bacillus licheniformis
Pseudoxanthomonas suwonensis
Candidomonas bauzanensis
Kaistia adipata
Cellulosimicrobium cellulans
Chryseobacterium wanjuense
B
Bacillus drentensis
Flavobacterium hauense
OD600
Time (h)

371

372 **Figure 5. *Rosellinia necatrix* culture filtrates inhibit the growth of particular**
373 **plant-associated bacterial species.** (A) Bacterial growth was measured over time
374 in *R. necatrix* culture filtrates, which were obtained after 4 (red), 7 (grey) and 9
375 (green) days of fungal growth. Heat-inactivated culture filtrates collected after 4
376 (blue), 7 (yellow) and 9 (black) days of fungal growth were used as controls. (B)
377 Growth of *Bacillus drentensis* and *Flavobacterium hauense* was measured upon
378 passing the culture filtrates collected after 4 (red), 7 (grey) and 9 (green) days of
379 fungal growth through spin-columns with 3 kDa cut-off (black, light green and pink,
380 respectively). The experiment was performed twice and error bars display standard
381 deviations (n=3).

382 **Table 3. Predicted secreted proteins of *R. necatrix* strain R18 with**
383 **structural homology to known antimicrobial proteins.**

R. necatrix gene ID	SignalP prediction confidence[a]	Structural homolog[b]	Prediction confidence (%)	Alignment coverage (%)[c]	Homolog protein size (kDa)[d]	Cys (%)[e]	pI[f]
FUN_000307	96.4	Bacterial enterotoxin	38.6	14	22.2	2.8	4.86
FUN_000408	99.3	Toxin	100	64	40.7	3.8	5.68
FUN_000625	99.3	Peptidoglycan-binding	100	98	12.3	4.5	8.79
FUN_000907	98.4	Toxin	40.1	35	28	2.6	5.03
FUN_001825	99.9	Hydrolase	100	95	38.4	1.8	5.11
FUN_001865	98.7	EGF/Laminin	91.4	13	34.6	3.6	7.01
FUN_002055	99.7	Endoglucanase	100	89	28.6	5.9	6.73
FUN_003304	99.3	Hydrolase	100	96	39.2	2.4	5.68
FUN_003451	99.1	Fungal ribonucleases	100	92	14.7	3.6	4.19
FUN_004580	99.8	Antifungal protein AFP1	55.5	6	47	2.5	4.85
FUN_004961	97.4	Toxin	25.2	23	19.7	3.8	7.75
FUN_005431	94.8	Thermolabile hemolysin	100	99	32.4	0.8	4.36
FUN_005483	99.6	NLP	100	87	28.9	3.3	4.87
FUN_005751	98.4	Fungal ribonuclease	100	93	14.4	3.6	6.05
FUN_005940	99.4	Toxin	40.6	17	13.9	5.8	6.63
FUN_006760	86.2	Carboxypeptidase	100	92	60.9	1.5	5.11
FUN_007808	91.5	Toxin	100	55	89	5.8	5.36
FUN_007991	98.2	Toxin	45.1	26	19	2.6	9.00
FUN_008352	99.6	Toxin	100	99	16.9	6.2	6.14
FUN_009115	96.1	Antimicrobial MIAMP1	87.8	33	24	3.2	4.65
FUN_009151	84.6	Phage lysozyme	100	94	20.7	3.6	6.92
FUN_009266	92.6	Neutrophil defensin 4	44.9	10	15.6	3.3	7.59
FUN_010039	97.8	Toxin	100	99	17.0	4.5	6.73
FUN_010165	99.5	Toxin	50.3	11	17.5	5.8	4.83
FUN_011519	98.6	Antimicrobial protein	15.2	57	5.8	5.7	4.78
FUN_011592	92.8	Defensin	49.9	10	18.8	6.7	7.41

384 [a]Secreted protein prediction confidence based on SignalP Version 5.0 (Almagro et al., 2019).
385 [b]Structural homology was determined based on Phyre2 prediction (Kelley et al., 2015).
386 [c]Alignment coverage of the *R. necatrix* gene query to the database homolog (subject).
387 [d]Protein size expressed in kilodaltons (kDa) of the database homolog.
388 [e]Amount of cysteines (Cys) present in the database homolog expressed in percentage (%).
389 [f]Isoelectric point (pI) of the database homolog.
390

391 **Prediction of potential antimicrobial effector candidates**

392 We previously showed that structural prediction successfully identified
393 antimicrobial effector proteins encoded in the genome of *V. dahliae* (Snelders et
394 al., 2020; 2021). Thus, we similarly mined the secretome of the *R. necatrix*
395 strain R18 for structural homologues of known antimicrobial proteins using
396 Phyre2 (Snelders et al., 2020; Kelley et al., 2015), leading to the identification of
397 26 candidates with potential antimicrobial activity (Table 3). Subsequently, we
398 used publicly available RNAseq data (Shimizu et al., 2018) to assess expression
399 of these candidates and found that nine of the 26 candidates are highly
400 expressed during avocado colonization (Fig. 6A). To further assess *in planta*
401 expression of the nine candidates, we measured their expression in *R. necatrix*
402 strain R18 upon cotton inoculation, revealing that five genes are highly
403 expressed during cotton colonization (Fig. 6B). To test whether these *in planta*-
404 expressed predicted secreted proteins indeed possess antimicrobial activity, we
405 pursued heterologous protein production in *E. coli*. Unfortunately, we repeatedly
406 failed to produce four of these proteins (FUN_009266, FUN_0100039,
407 FUN_005751 and FUN_006760) which, although it may be interpreted as a sign
408 of potential antimicrobial activity (Ingham and Moore, 2007), obstructs functional
409 analysis. However, one protein could be successfully produced and purified
410 (FUN_004580).

411 FUN_004580 has predicted structural homology to antifungal protein 1
412 (AFP1) from the bacterium *Streptomyces tendae* (Campos-Olivas et al., 2001)
413 (Figure 7A,B). This protein was identified in a screen for antifungal activity as a
414 non-enzymatic chitin-binding antifungal directed against particular Ascomycete
415 fungi (Bormann et al., 1999). Intriguingly, attempts to produce functional AFP1
416 in the lactic acid bacterium *Lactococcus lactis* failed (Freitas et al., 2005),

417 suggesting that the protein may exert antibacterial activity as well. BLAST
418 searches using the FUN_004580 amino acid sequence revealed ~100
419 Ascomycete fungal homologs, while HMMER searches revealed homologs in the
420 Streptophyta clade (Viridiplantae) too (Supplemental Table 6). Interestingly,
421 BLAST and HMMER searches using the amino acid sequence of FUN_004580 did
422 not reveal homology to AFP1, underpinning that structural homology, rather than
423 sequence homology, drove the prediction of FUN_004580 as an antimicrobial.

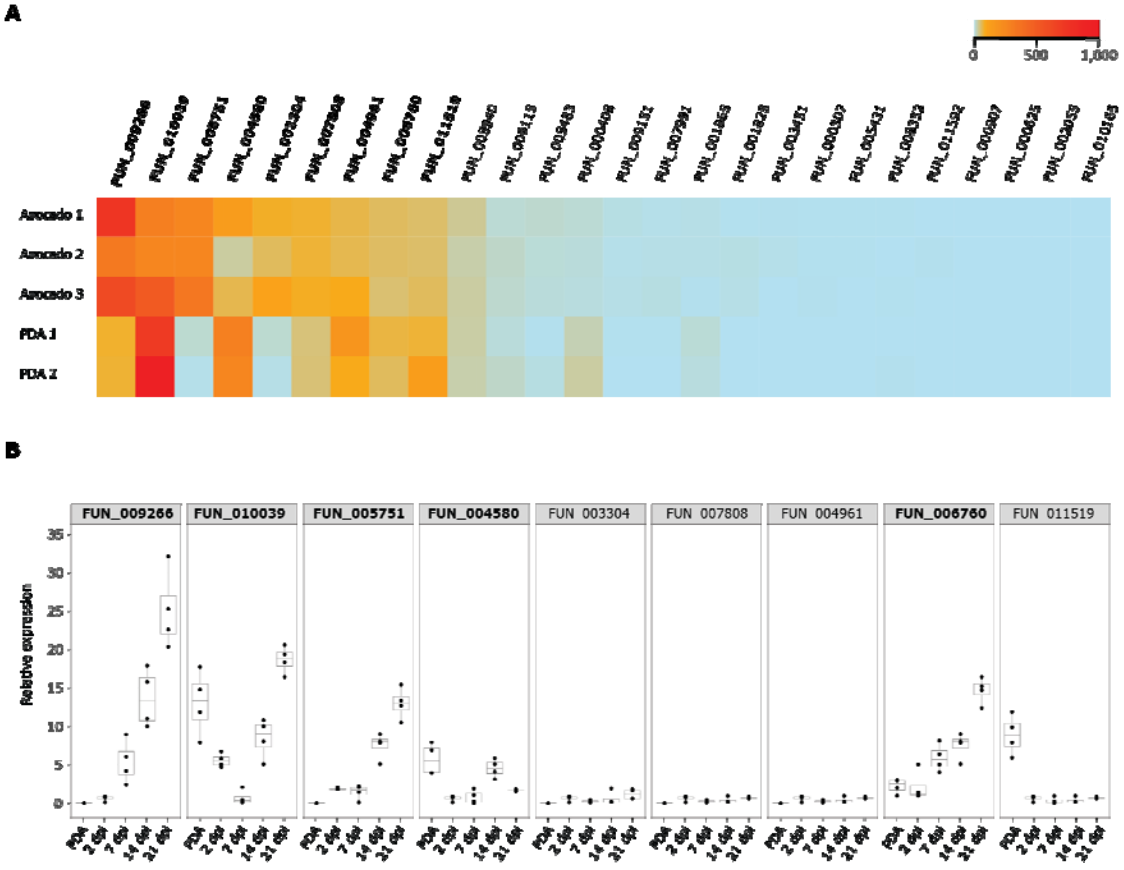

424

425 **Figure 6. *In planta* expression of *Rosellinia necatrix* genes predicted to**
426 **encode effector proteins with antimicrobial activity.** (A) *In silico* analysis of
427 publicly available RNAseq data of avocado plants infected with *R. necatrix* (n=3)
428 reveals nine genes that are highly induced *in planta* (shown in bold) out of 26 that
429 encode potential antimicrobial proteins (AMPs). Several of these are also expressed
430 upon cultivation of *R. necatrix in vitro* on potato dextrose agar (PDA) (n=2). (B)
431 Real-time PCR of nine *in planta* expressed *R. necatrix* genes identified in (A) reveals
432 that five genes are expressed during cotton colonization at 14 and 21 days post
433 inoculation (shown in bold).

434

435 An alternative manner to obtain proteins for functional analysis that does
436 not rely on expression in heterologous microbial expression systems is peptide
437 synthesis, although this is typically limited to sequences shorter than 100 amino
438 acids. Unfortunately, all five effectors that are expressed in cotton are larger
439 than this size. However, among the nine candidates that are highly expressed
440 during avocado colonization, one encodes a protein (FUN_011519) small enough
441 for protein synthesis (Biomatik Corporation, Ontario, Canada).

442 FUN_011519 has predicted structural homology to the antimicrobial
443 protein AcAMP2 from the plant *Amaranthus caudatus* (Martins et al., 1996)
444 (Figure 7C,D). This protein was identified based on homology to cysteine/glycine-
445 rich domain of plant chitin-binding proteins and showed antifungal activity, as
446 well as activity against Gram-positive bacteria (Broekaert et al., 1992). BLAST
447 and HMMER searches revealed only Ascomycete fungal homologs, identifying
448 ~100 fungal proteins (Supplemental Table 7). Interestingly, BLAST and HMMER
449 searches using the amino acid sequence of FUN_011519 did not reveal homology
450 to AcAMP2, underpinning that also in this case structural homology, rather than
451 sequence homology, drove the prediction as antimicrobial.

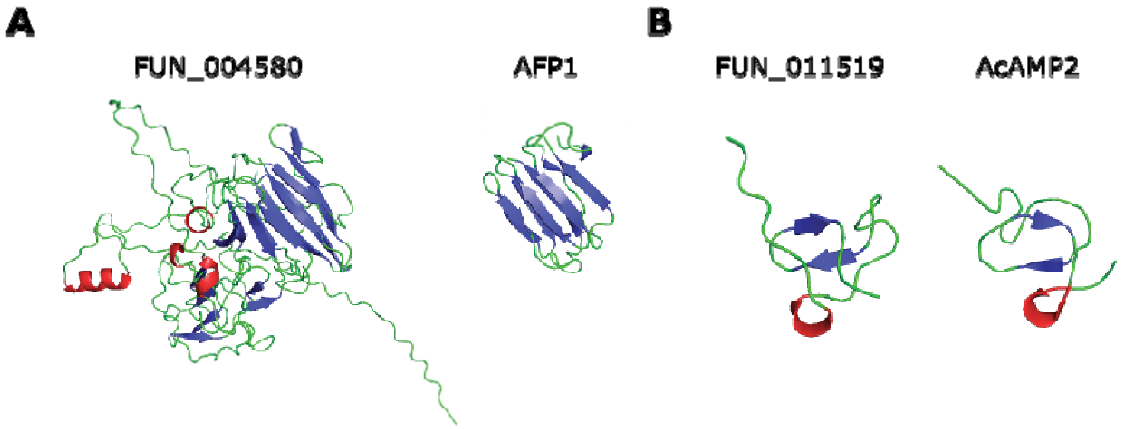

452

453 **Figure 7. *Rosellinia necatrix* effector proteins with predicted antimicrobial**
454 **activity based on structural homology.** (A) Alphafold2 model of *R. necatrix*

455 effector protein FUN_004580 (left) shows structural homology to antifungal protein 1
456 (AFP1) from the bacterium *Streptomyces tendae* (right). (B) Alphafold2 model of *R.*
457 *necatrix* effector protein FUN_011519 (left) shows structural homology to
458 antimicrobial protein AcAMP2 from the plant *Amaranthus caudatus* (right).

459

460 **Candidate antimicrobial effector proteins display selective antimicrobial**
461 **activity**

462 Given that FUN_004580 and FUN_011519 were identified based on structural
463 homology to proteins with antifungal activity, we tested potential antimicrobial
464 activity on eight fungal species: five filamentous fungi (*Verticillium dahliae*,
465 *Alternaria brassicicola*, *Cladosporium cucumerinum*, *Trichoderma viridae* and *R.*
466 *necatrix*), and four yeasts (*Pichia pastoris*, *Cyberlindnera jadinii*, *Debaryomyces*
467 *vanrijiae* and *Rhodorotula bogoriensis*). Interestingly, both proteins displayed
468 selective antifungal activity. Whereas FUN_004580 inhibited the growth of all
469 filamentous fungi tested, except *R. necatrix* (Fig. 7A) as well as of all yeasts
470 except *P. pastoris* (Fig. 7B), FUN_011519 had a narrower activity spectrum as it
471 only inhibited the growth of *V. dahliae* and *A. brassicicola* (Fig. 7C), and the
472 yeasts *C. jadinii* and *R. bogoriensis* (Fig. 7D). Thus, we conclude that both
473 proteins possess clear antifungal activity.

474 To further investigate the antimicrobial activity of the two predicted
475 secreted effector proteins FUN_004580 and FUN_011519, we tested their activity
476 on the diversity panel of 37 bacteria that span a wide range of taxonomic
477 diversity, including Gram-positive and Gram-negative taxa (Table 5).
478 Interestingly, although we found that the growth of most bacteria was not
479 affected by any of the two proteins, growth of some bacteria was clearly
480 hampered. Whereas FUN_004580 strongly impacted growth of
481 *Pseudoxanthomonas suwonensis*, *Flavobacterium hauense*, and
482 *Cellulosimicrobium cellulans*, and inhibited *Chryseobacterium wanjuense* to a

483 lesser extent, FUN_011519 inhibited *Bacillus drentensis* and *Achromobacter*
484 *denitrificans*, and possibly also *Sphingobium mellinum* and *Candidimonas*
485 *bauzanensis* (Fig. 8). Thus, we conclude that both effectors display antibacterial
486 activity as well. Collectively, our data show that both effector proteins possess
487 selective antimicrobial activity.

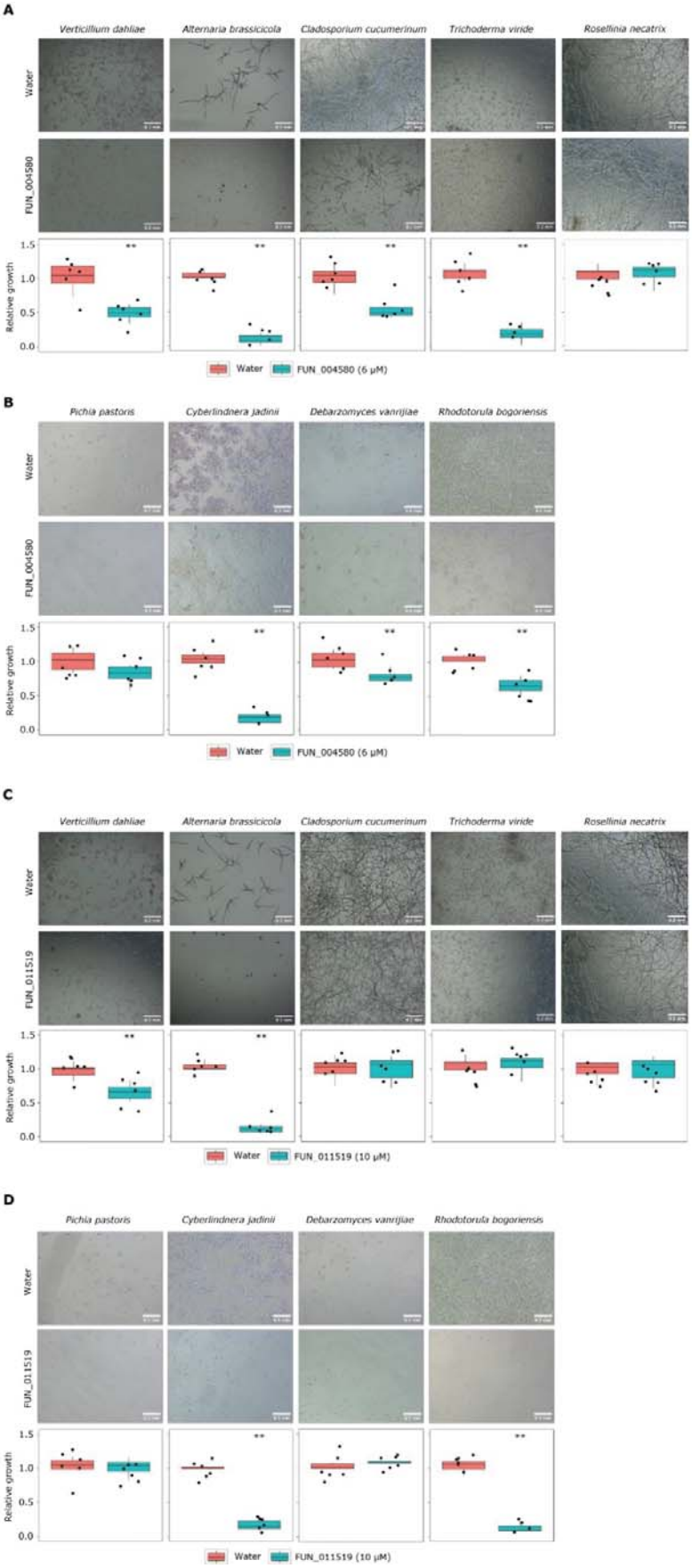
A
Verticillium dahliae
Alternaria brassicicola
Cladosporium cucumerinum
Trichoderma viride
Rosellinia necatrix
Water
FUN_004580
Relative growth
1.5
1.0
0.5
0.0
**
Water
FUN_004580 (6 μM)
B
Pichia pastoris
Cyberlindnera jadinii
Debarzomyces vanrijiae
Rhodotorula bogoriensis
Water
FUN_004580
Relative growth
1.5
1.0
0.5
0.0
**
Water
FUN_004580 (6 μM)
C
Verticillium dahliae
Alternaria brassicicola
Cladosporium cucumerinum
Trichoderma viride
Rosellinia necatrix
Water
FUN_011519
Relative growth
1.5
1.0
0.5
0.0
**
Water
FUN_011519 (10 μM)
D
Pichia pastoris
Cyberlindnera jadinii
Debarzomyces vanrijiae
Rhodotorula bogoriensis
Water
FUN_011519
Relative growth
1.5
1.0
0.5
0.0
**
Water
FUN_011519 (10 μM)

488

489 **Figure 8. *Rosellinia necatrix* effector proteins display antifungal activity.**
490 Fungal growth in 5% potato dextrose broth (PDB) in presence of FUN_004580 (6 µM)
491 or water of filamentous fungal species (A) and yeasts (B), or in presence of
492 FUN_011519 (10 µM) or water of filamentous fungal species (C) and yeasts (D).
493 Relative growth as display in microscopic pictures (n=6) was quantified using
494 ImageJ. Asterisks indicate significant differences (unpaired two-sided Student's t test
495 (P<0.01)).

496

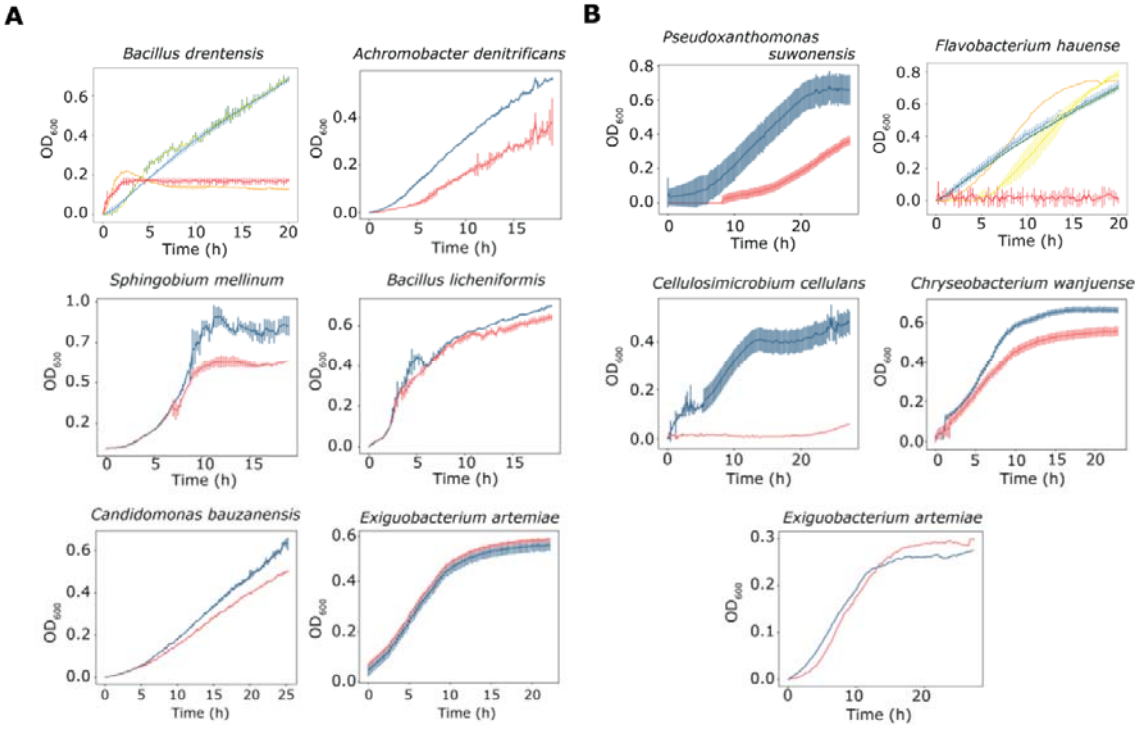

497

498 **Figure 9. *Rosellinia necatrix* effector proteins display selective antimicrobial**
499 **activity against plant-associated bacteria.** (A) Red lines show bacterial growth in
500 presence of FUN_011519 (10 µM) while blue lines show bacterial growth in water.
501 For *Bacillus drentensis* additional orange line shows bacterial growth in protein
502 filtered with spin-column with 10 kDa cut off, green line shows bacterial growth in
503 protein filtered with spin-column with 3 kDa cut off, and yellow line shows growth in
504 heat-inactivated protein. (B) Red lines show bacterial growth in presence of
505 FUN_004580 (6 µM) while blue lines show bacterial growth in water. For
506 *Flavobacterium hauense* additional orange line shows bacterial growth in protein
507 filtered with spin-column with 10 kDa cut off, green line shows bacterial growth in
508 protein filtered with spin-column with 3 kDa cut off, and yellow line shows growth in
509 heat-inactivated protein. Error bars display standard deviations (n=3). Growth of
510 *Exiguobacterium artemiae* is not inhibited by either protein and is shown as a
511 representative of non-inhibited bacterial taxa.

512

513 **Several plant-associated bacteria display antagonistic activity**

514 One obvious reason for a fungus to target particular microbes with antimicrobials
515 is that these may be detrimental to fungal growth due to the display of
516 antagonistic activities. To test for such activities directed against *R. necatrix*, we
517 conducted confrontation assays *in vitro*, where we grew *R. necatrix* near the
518 individual bacteria species from the diversity panel of 37 bacteria (Table 5). In
519 these assays, we observed antagonistic effects of several bacterial species on *R.*
520 *necatrix* (Fig. 10). Interestingly, several of the bacterial species inhibited by
521 either of the two effector proteins displayed antagonistic activity against *R.*
522 *necatrix*, including *Bacillus drentensis*, *Bacillus licheniformis*, and *Sphingobium*
523 *mellinum* (inhibited by FUN_011519), and *Cellulosimicrobium cellulans*,
524 *Chryseobacterium wanjuense* and *Pseudoxanthomonas suwonensis* (inhibited by
525 protein FUN_004580) (Fig. 10). However, also some other bacterial species that
526 were not found to be inhibited by either of the two effector proteins displayed
527 antagonistic activity, namely *Kaistia adipata, Pedobacter steynii, Pedobacter*
528 *panaciterrae, Pseudomonas corrugata, Pseudomonas knackmusii, Solibacillus*
529 *isronensis* and *Solibacillus silvestris*. These findings suggest that a diversity of
530 plant-associated bacteria possess inherent antagonistic activity against *R.*
531 *necatrix* and that some of these bacteria are targeted by effector proteins of *R.*
532 *necatrix.*
533

534 **Particular antagonists alleviate Rosellinia disease in cotton**

535 To test whether any of the bacterial species that are inhibited by the *R. necatrix*
536 effector proteins and that display antagonistic activity against the fungus can
537 inhibit disease development, we pursued inoculation assays in the presence and
538 absence of these bacteria. As *R. necatrix* is a broad host range pathogen, we
539 performed infection assays on cotton plants. To this end, 14-day-old cotton cv.

540 XLZ seedlings were inoculated with *R. necatrix* strain R18, leading to clear
541 disease symptoms by two weeks after inoculation (Fig. 11). Next, we pre-treated
542 cotton cv. XLZ seeds with antagonistic bacteria *Bacillus drentensis*, *Sphingobium*
543 *mellinum*, *Cellulosimicrobium cellulans*, or *Pseudoxanthomonas suwonensis*. To
544 show that the inhibition of disease development by the antagonistic bacteria is
545 not caused by the activation of MAMP-triggered host immunity we included pre-
546 treatment with the non-antagonistic bacteria *Exiguobacterium artemiae*,
547 *Candidomonas bauzanensis*, *Flavobacterium hauense*, *Achromobacter*
548 *denitrificans*, or soil. Furthermore, a mix of all bacteria including the antagonistic
549 and non-antagonistic bacteria species was included as well as water as a control,
550 followed by *R. necatrix* inoculation. Interestingly, two weeks after inoculation it
551 could be observed that pretreatment with each of the antagonistic bacteria
552 resulted in reduced susceptibility of the cotton plants to *R. necatrix* when
553 compared with the plants that did not receive a bacterial pre-treatment. Because
554 treatment with the non-antagonistic bacterial species or soil suspension did not
555 lead to reduced disease symptoms, we infer that the reduced disease
556 development upon treatment with then antagonistic bacteria is unlikely to be
557 caused by the activation of MAMP-triggered host immunity, but rather likely
558 through direct antagonism towards the fungal pathogen. Finally, none of the
559 bacteria affected growth of the cotton plants in absence of pathogen inoculation
560 (Fig. 11).

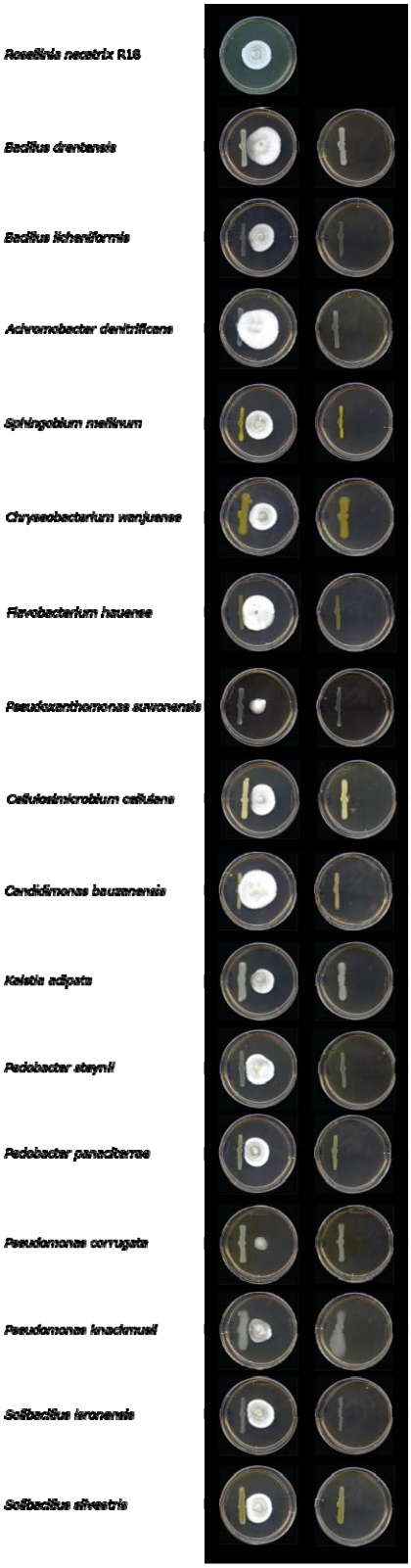

Figure 10. **Various plant-associated bacteria display antagonistic activity against R*osellinia necatrix*.** Fungal PDA disks were placed in the center of a petri dish and next to it individual bacteria species were deposited in a straight line with

help of a spreader (n=5), bacteria species were placed alone (right column) as controls.

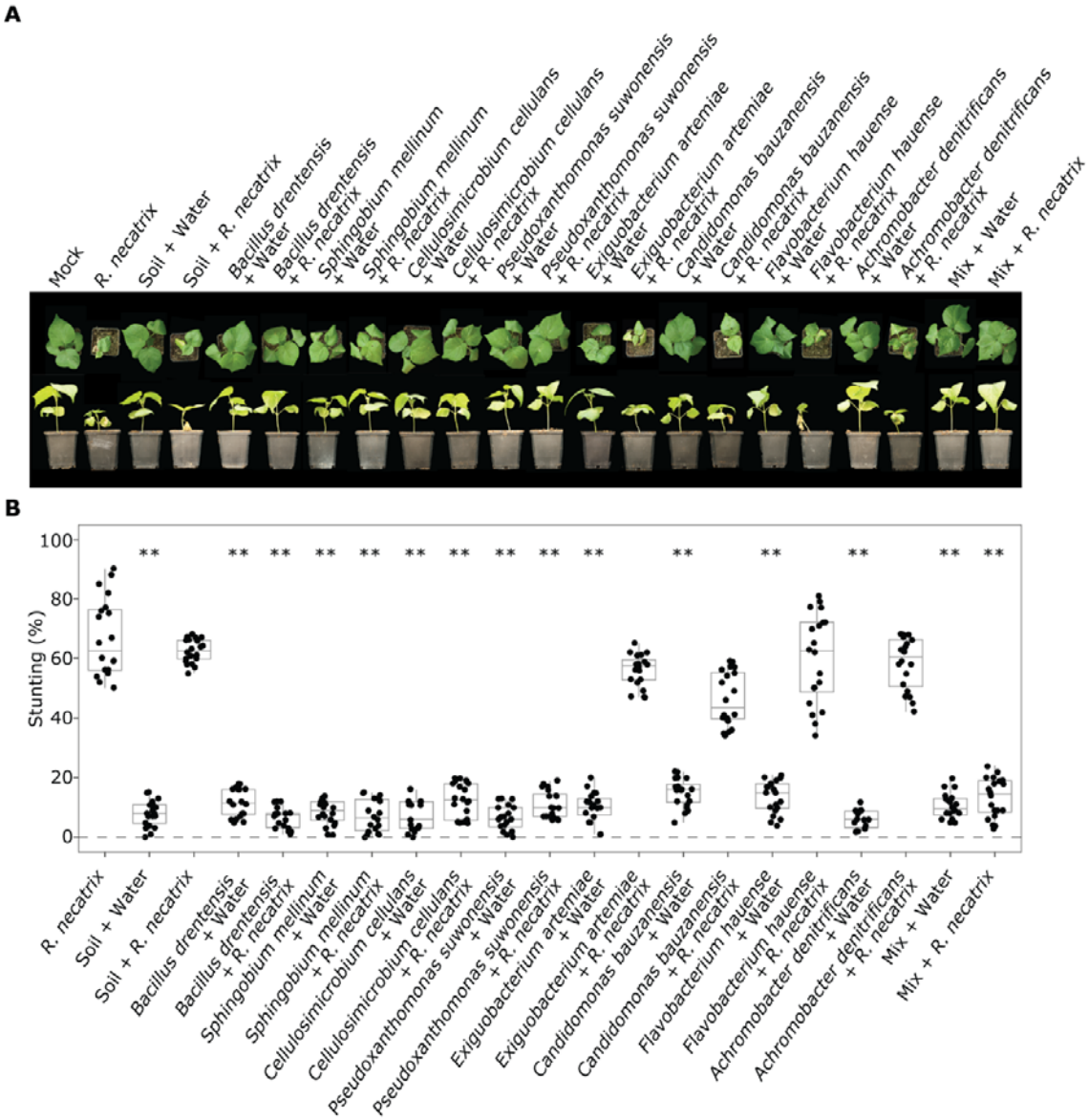

Figure 11. **Antagonistic plant-associated bacteria reduce white root rot disease in cotton.** (A) Top and side pictures of cotton plants. Cotton seeds were soaked in a suspension of the antagonistic bacteria *Bacillus drentensis*, *Sphingobium mellinum*, *Cellulosimicrobium cellulans*, or *Pseudoxanthomonas suwonensis*, and the non-antagonistic bacteria *Exiguobacterium artemiae*, *Candidomonas bauzanensis*, *Flavobacterium hauense*, or *Achromobacter denitrificans*, a mix of all bacteria, soil suspension, or water as a control. Subsequently, germlings (n=10) were inoculated with *R. necatrix* strain R18 or mock-inoculated. (B) Quantification of stunting. Asterisks indicate significant differences between *R. necatrix*-inoculated plants and plant seeds treated with bacteria (ANOVA followed by Fisher's LSD test ($P<0.01$)). The experiment was performed twice.

579 **DISCUSSION**

580 Increasing evidence supports the notion that plants can recruit microbes into
581 their microbiota that can help them to withstand pathogen infection (Wang et al.,
582 2012; Pérez-Jaramillo et al., 2016; Zhalnina et al., 2018; Chai and Schachtman,
583 2022). Based on this notion, it has been hypothesized that pathogens have
584 evolved to counter-act the recruitment of beneficial microbes to promote host
585 colonization (Snelders et al., 2018). In support of this hypothesis, it has been
586 shown that the soil-borne fungal pathogen *Verticillium dahliae* secretes a suite of
587 effector molecules with selective antimicrobial activities to suppress antagonistic
588 microbes in host microbiota to support host ingress (Snelders et al. 2020; 2021;
589 2022). Although it has been hypothesized that other fungal pathogens are likely
590 to have evolved to modulate host microbiota as well (Snelders et al. 2020;
591 Snelders et al. 2022), evidence for this hypothesis has been lacking thus far. In
592 this study, we show that the soil-borne pathogen *Rosellinia necatrix* similarly
593 expresses predicted secreted effector proteins during host colonization with
594 selective antimicrobial activity. Specifically, we show that two genes encoding
595 the effector proteins, FUN_004580 and FUN_011519, are expressed during host
596 colonization and these predicted secreted effectors display selective antimicrobial
597 activity *in vitro* towards specific plant-associated bacteria and fungi. Intriguingly,
598 some of the bacterial species that are inhibited by the antimicrobial effector
599 proteins display antagonistic activity towards *R. necatrix in vitro*. Moreover, when
600 applied to cotton seeds, several of the antagonistic bacterial species reduce white
601 root rot disease. Collectively, our findings suggest that *R. necatrix* secretes
602 antimicrobial effector proteins during host colonization to modulate host
603 microbiota and support disease development.

604 The effector proteins FUN_004580 and FUN_011519 were found based on
605 structural homology to AFP1 from the bacterium *Streptomyces tendae* and
606 homology to AcAMP2 from the plant *Amaranthus caudatus*, respectively. AFP1
607 has been described as a non-enzymatic chitin-binding antifungal directed against
608 particular Ascomycete fungi (Bormann et al., 1999), and recent studies have
609 shown that a homolog of AFP1 isolated from the plant *Carum carvi* (Cc-AFP1)
610 alters fungal cell membrane permeability (Sadat et al., 2021). AcAMP2 was
611 identified based on homology to cysteine/glycine-rich domain of plant chitin-
612 binding proteins and showed antifungal activity, as well as activity against Gram-
613 positive bacteria (Broekaert et al., 1992). The antimicrobial mechanism
614 described for the structural homologs suggest that FUN_004580 and
615 FUN_011519 could potentially be involved in cell membrane disruption, but
616 further functional studies that also include antifungal activity assays are required
617 to investigate this.

618 The effector proteins FUN_004580 and FUN_011519 showed selective
619 antimicrobial activity against plant-associated bacterial and fungal species *in*
620 *vitro* and display divergent activity spectra, suggesting that they possess additive
621 activities. Similar observations have been made for the antimicrobial effector
622 proteins VdAMP2 and VdAve1 of *V. dahliae* that add to each other's activity
623 spectra during soil colonization (Snelders et al., 2020). Divergent activity spectra
624 have been also observed in the *in planta*-expressed effectors VdAve1, VdAve1L2
625 and VdAMP3 (Snelders et al., 2020; 2022). Furthermore, differential expression
626 of antimicrobial effectors on different plant hosts was observed in *R. necatrix*.
627 Out of the 26 AMP candidates, nine are expressed during avocado colonization,
628 and five of them were also expressed during cotton colonization. From these,
629 *FUN_004580* and *FUN_011519* are expressed during avocado colonization, while

630 only *FUN_004580* is expressed on cotton (Fig. 4). The expression profiles on
631 different host plants suggest differential expression of antimicrobials in *R.*
632 *necatrix*, potentially due to differential microbiota compositions of these plant
633 hosts. Possibly, FUN_011519 evolved to target microbes that are specifically
634 associated with avocado, or absent from the microbiota of cotton plants.

635 Various studies have shown that plants shape their microbiota composition
636 (Berendsen et al., 2012). For example, one single gene responsible for the
637 production of glucosinolate significantly altered the microbial community on the
638 roots of transgenic *Arabidopsis* (Bressan, 2009). Moreover, the ATP-binding
639 cassette (ABC) transporter *abcg30* mutant of *Arabidopsis thaliana* secretes root
640 exudates that are enriched in phenolic compounds and contain fewer sugars,
641 resulting in distinct root microbiota compositions (Badri and Vivanco, 2009).
642 Furthermore, *A. thaliana* genes responsible for defense, kinase-related activities,
643 and cell wall integrity impact the microbiota composition (Beilsmith et al., 2019).
644 Besides *A. thaliana*, different potato and tomato plants assemble different
645 microbiota compositions (Weinert et al., 2011; Cordovez et al., 2021).

646 Like *V. dahliae*, *R. necatrix* is a soil-borne pathogen that resides for part of
647 its life cycle in the microbe-rich soil where inter-microbial competition for limited
648 nutrients is ferocious. Although *R. necatrix* is phylogenetically related to *V.*
649 *dahliae*, both belonging to the class of Sordariomycetes, our findings suggest
650 that exploitation of antimicrobial effector proteins among soil-borne fungi may be
651 commonplace. However, whether the employment of such effector proteins is
652 relevant for soil-borne pathogens only, or shared by other types of plant
653 pathogens too, presently remains enigmatic (Snelders et al., 2022a).

654 To further investigate the effector catalog of *R. necatrix*, we investigated
655 whether effector genes in *R. necatrix* are associated with repetitive regions. The

656 genomes of many filamentous plant pathogens are compartmentalized,
657 comprising gene-dense/repeat-poor regions harboring essential and widely
658 conserved housekeeping genes and gene-sparse/repeat-rich regions containing
659 fast-evolving virulence-associated genes (Rafaelle et al., 2010; Dong et al.,
660 2015; Frantzeskakis et al., 2020). However, in the case of *R. necatrix*, the repeat
661 content is low, and interestingly, the vast majority of repetitive elements are not
662 located in close proximity to effectors. This suggests that effector genes in *R.*
663 *necatrix* are not associated with repeat-rich regions. Similar to *R. necatrix*, other
664 genomes have been found to lack obvious genome compartmentalization such as
665 that of the leaf spot fungus *Ramularia collo-cygni* (Stam et al., 2018), the barley
666 powdery mildew fungus *Blumeria graminis* f.sp. *hordei* (Frantzeskakis et al.,
667 2018) and the wheat stripe rust fungus *Puccinia striiformis* f.sp. *tritici*
668 (Schwessinger et al., 2018). Intriguingly, while the genome of the latter two is
669 characterized by a high repeat content, the genome of *Ramularia collo-cygni* has
670 a low repeat content like *R. necatrix* (Stam et al., 2018; Frantzeskakis et al.,
671 2018; Schwessinger et al., 2018). In such genomes, adaptation and evolution of
672 effector genes were suggested to be governed by copy-number variation (CNV)
673 and heterozygosity of the effector loci (Frantzeskakis et al., 2018). In *R.*
674 *necatrix,* we showed that insertions and deletions are predominant structural
675 variants (SVs) that are associated with effector genes, which suggests that these
676 SVs may play a role in evolution of the effector catalog.

677 To understand the diversity and functional properties of effectors, we
678 investigated their 3D protein structure. The results of this study demonstrate
679 that there is relatively little structural clustering among *R. necatrix* effectors. The
680 five largest clusters identified were mainly driven by sequence conservation
681 rather than structural similarity, suggesting that effector family expansion based

682 on structural similarity played only a minor role in *R. necatrix* effector evolution.
683 Effector protein structure clustering has revealed that many plant pathogen
684 effectors fall into distinct structural families. For example, MAX (de Guillen et al.,
685 2015), and RNase-Like proteins associated with haustoria (RALPH) (Spanu,
686 2017) are effector families with structural similarity. Common themes are
687 emerging like structural homology and in some cases similar modes of action (Lu
688 et al., 2015). While structural conservation has been observed in some
689 pathogenic fungi (de Guillen et al., 2015; Spanu, 2017), sequence conservation
690 is the main driver of structural clustering among *R. necatrix* effectors. Future
691 studies could explore the functional significance of the identified effector clusters
692 in *R. necatrix* and other plant pathogens and investigate the mechanisms
693 underlying the evolution of effector proteins.

694 **MATERIALS AND METHODS**

695 **Nanopore sequencing and genome assembly**

696 High-molecular weight (HMW) DNA was extracted from nine *R. necatrix* strains
697 (Table 1) as described by Chavarro-Carrero et al. (2021), except that mycelium
698 was grown in 1/5 PDB instead of Czapek Dox medium. DNA quality, size and
699 quantity were assessed with Nanodrop, Qubit analyses, and with gel
700 electrophoresis. Library preparation with the Rapid Sequencing Kit (SQK-
701 RAD004) was performed with ~400 ng HMW DNA according to the
702 manufacturer's instructions (Oxford Nanopore Technologies, Oxford, UK). An
703 R9.4.1 flow cell (Oxford Nanopore Technologies, Oxford, UK) was loaded and ran
704 for 24 h, and subsequent base calling was performed using Guppy (version
705 3.1.3; Oxford Nanopore Technologies, Oxford, UK). Adapter sequences were
706 removed using Porechop (version 0.2.4 with default settings; Wick, 2018) and
707 the reads were self-corrected, trimmed and assembled using Canu (version 1.8;
708 Koren et al., 2017).

709 To obtain longer reads ultra-high-molecular weight (UHMW) DNA
710 extraction was performed. To this end, after DNA precipitation, the Nanobind Big
711 DNA Kit (SKU NB-900-801-01, Circulomics, USA) was used following the
712 manufacturer's protocol to select DNA fragments >50 kb. Simultaneously, to
713 allow error correction of the ONT reads, paired-end short read (150 bp)
714 sequencing was performed at the Beijing Genome Institute (BGI) using the
715 DNBseq platform. After error correction using FMLRC (version 1.0.0 with default
716 settings; Wang et al., 2018), ONT reads were trimmed and assembled using
717 Canu.

718 Hi-C was performed based on the Proximo Hi-C kit (Microbe) (Phase
719 Genomics, Seattle, WA, USA) according to the manufacturer's protocol as

720 previously described (Seidl et al., 2020), and the Hi-C library was paired-end
721 (150 bp) sequenced on the NextSeq500 platform at USEQ (Utrecht, the
722 Netherlands). Subsequently, Hi-C reads were mapped to the Canu assembly
723 using Juicer (version 1.6 with early-stage setting; Durand et al., 2016), and the
724 three-dimensional (3D) *de novo* assembly (3D-DNA) pipeline (version 180922
725 with contig size threshold 1000; Dudchenko et al., 2017) was used. The genome
726 assembly was further manually improved using Juicebox Assembly Tools (JBAT)
727 (version 1.11.08; Dudchenko et al., 2018) and the 3D-DNA post review asm
728 pipeline (Dudchenko et al., 2017). Tapestry (version 1.0.0 with default settings;
729 (Davey et al., 2020) was used to visualize chromosomes and telomeric regions
730 with telomeric sequence ([TTAGGG]*n*).
731

732 **Phylogenetic tree construction and structural variant calling**

733 A phylogenetic tree of all sequenced strains was constructed with Realphy
734 (version 1.12) (Bertels *et al.,* 2014). Briefly, genomic reads were mapped
735 against the genome of strain R18 using Bowtie2 (version 2.2.6) (Langmead and
736 Salzberg, 2012) and a maximum-likelihood phylogenetic tree was inferred using
737 RAxML (version 8.2.8) (Stamatakis, 2014), using the genome sequence of
738 *Rosellinia corticium* to root the tree. Subsequently, to predict SVs, we used
739 NanoSV (version 1.2.4 with default settings; Stancu et al., 2017) for each of the
740 genomes when compared to R18 strain as reference. The output of each strain
741 was initially filtered with bcftools v.1.3.2 using GT=AA, QUAL>50, GQ>10,
742 SUPPORT>20 (Danecek et al., 2021). The results were merged using SURVIVOR
743 v.1.0.6 (Jeffares et al., 2017), allowing 1,000 bp as the maximum distance for
744 breakpoints and considering only same SV types. Only SVs with minimum size
745 >100 bp and maximum size of 100 kb were kept. Permutation tests were

746 computed using R/Bioconductor region v.1.8.1 package (Gel et al., 2016), and
747 10,000 iterations were performed using the mean distance to evaluate the
748 closest relationship (bp distance) between SV-breakpoints, TEs and effectors,
749 and circular randomization as well to maintain the order and distance of the
750 regions on the chromosomes.
751
752 **Genome mining**
753 Genome annotation was performed using Funannotate (Version 1.8.13, Palmer
754 and Stajich, 2017) guided by publicly available RNAseq data (Shimizu et al.,
755 2018). Furthermore, secreted genes, effector genes and secondary metabolite
756 gene clusters were predicted using SignalP (Version 5.0, Almagro et al., 2019),
757 EffectorP (Version 2.0, Sperschneider et al., 2018) and antiSMASH (Version
758 6.0.0, Blin et al., 2019), respectively. The *R. necatrix* R18 genome was mined for
759 gene candidates that encode secreted antimicrobials as described previously
760 (Snelders et al., 2020). Briefly the predicted secretome and effector catalog were
761 mined using Phyre2 (Kelley et al., 2015), followed by manual curation, to search
762 for predicted structural homologues of known antimicrobial proteins. Gene
763 sequences were extracted using Bedtools (setting: getfasta) (Quinlan and Hall,
764 2010). Subsequently, RNAseq data were used to confirm expression of selected
765 candidates. To this end, RNAseq data was mapped to the R18 assembly and
766 relative expression was calculated using Kallisto (version 0.46.1, default settings,
767 Bray et al., 2016).
768 Repetitive regions were annotated using EDTA v.1.9.4 (Ou et al., 2019).
769 Briefly, we used the 'sensitive', 'anno' and 'evaluate' options to maximize the
770 transposable element discovery and integrity. Then, the TE library was refined

771 using one code to find them all (Bailly-Bechet et al., 2014), and only full LTRs
772 were kept.
773
774 **Structural prediction of the *R. necatrix* effector catalog**
775 Structural predictions of effector candidates were done based on mature amino
776 acid sequences, lacking signal peptides, with Alphafold2 (Jumper et al., 2021)
777 using the casp14 preset. Five models were generated for each effector candidate,
778 of which the one with the highest pLDDT score was used for further analysis. To
779 assess structural similarity between effector candidates, an all-vs-all alignment
780 was performed using TM-align (Zhang and Skolnick, 2005). Structures were
781 considered similar when the average TM-score of pairwise reciprocal alignments,
782 calculated on a 0-1 scale, was >0.5. Effector clusters were identified by simple
783 agglomerative hierarchical clustering based on structural similarity using SciPy
784 (Virtanen et al., 2020) and a minimum similarity threshold of 0.5. For the five
785 largest clusters the average sequence identity was calculated from a multiple
786 sequence alignment performed with MAFFT on EMBL-EBI (Katoh and Standley,
787 2013). Cluster annotation was performed by generating PANNZER (Törönen and
788 Holm, 2022) annotation for each protein followed by manual curation of a
789 consensus annotation for each cluster. Protein structures were generated with
790 PyMOL (The PyMOL Molecular Graphics System, Version 2.0 Schrödinger, LLC,
791 DeLano Scientific, Palo Alto, CA, USA).
792
793 **Real-time PCR**
794 To determine expression profiles of candidate genes that encode secreted
795 antimicrobials during *R. necatrix* infection of cotton, two-week-old cotton (cv.
796 XLZ) seedlings were inoculated, as previously described (Cazorla et al., 2006),

797 with *R. necatrix* strain R18, and stems were harvested up to 21 dpi.
798 Furthermore, mycelium was harvested from ten-day-old *R. necatrix* strain R18
799 cultures on potato dextrose agar (PDA) plates. Total RNA extraction and cDNA
800 synthesis were performed as previously described (Santhanam et al., 2013).
801 Real time-PCR was performed with primers listed in Supplemental Table 5, using
802 the *R. necatrix* glyceraldehyde-3-phosphate dehydrogenase gene (GAPDH;
803 FUN_007054) as endogenous control. The PCR cycling conditions consisted of an
804 initial 95°C denaturation step for 10 min followed by denaturation for 15□s at
805 95°C, annealing for 30□s at 60°C, and extension at 72°C for 40□cycles.
806

807 **Heterologous protein production**

808 The sequences encoding mature proteins were cloned into vector pET-15b with
809 an N-terminal His6 tag sequence (Novagen, Darmstadt, Germany) (primer
810 sequences, see Supplemental Table 5). The resulting expression vectors were
811 verified by sequencing and used to transform *Escherichia coli* strain BL21. For
812 heterologous protein production, BL21 cells were grown in 2× yeast extract
813 tryptone (YT) medium at 37°C with continuous shaking at 200 rpm until the
814 cultures reached an optical density measurement at 600 nm (OD_{600}) of 2. Protein
815 production was induced with 1 mM isopropyl β-D-1-thiogalactopyranoside (IPTG)
816 at 42°C and shaking at 200 rpm for 2 h. Bacterial cells were pelleted and washed
817 with 50mM Tris HCl and 10% glycerol at pH 8.0. To disrupt cells, they were
818 sonicated three times according to a cycle composed of one second sonication,
819 followed by 0.5 seconds on ice and a one-minute pause. Next, the samples were
820 centrifugated at 16,000g for 10 min. The insoluble pellets were resuspended in
821 30 mL of 6 M guanidine hydrochloride (GnHCl), 10 mM Tris at pH 8.0 and 10 mM
822 β-mercaptoethanol and incubated overnight at room temperature. Next, debris

823 was pelleted by centrifuging at 16,000g for 10 min and the resulting protein
824 solution was transferred to a new tube and filtered step-wise from 1.2 to 0.45
825 µm. Proteins were subsequently purified under denaturing conditions by metal
826 affinity chromatography using a pre-packed HisTrap FF column (Cytiva,
827 Medemblik, The Netherlands) and dialysed (Spectra/Por 3 Dialysis Membrane,
828 molecular weight cut off of 10 kDa; Spectrum Laboratories, Rancho Dominguez,
829 U.S.A) against 20 volumes of 0.01 M BisTris, 10 mM reduced glutathione and 2
830 mM oxidized glutathione at pH 8.0 with decreasing GnHCl concentrations in five
831 consecutive steps of minimum 24 h from 5 M to 1 M for refolding. Finally,
832 proteins were dialysed against demineralized water for 24 h and final
833 concentrations were determined using Qubit (ThermoFisher Scientific, Waltham,
834 U.S.A).
835
836 **Culture filtrate production**
837 *R. necatrix* strain R18 was grown in potato dextrose broth (PDB) at 21°C and
838 130 rpm. Cultures were collected at 4, 7 and 9 days after the start of incubation
839 and mycelium was separated from the culture medium using a 0.45 nm filter.
840 Half of the culture-filtrate was heat-inactivated at 96°C for 10 minutes. Finally,
841 culture filtrates were stored at -20°C until use.
842
843 ***In vitro* antimicrobial activity assays**
844 Growth assays were performed as previously described (Snelders et al., 2020).
845 Briefly, bacterial strains were grown overnight on lysogeny broth agar (LBA),
846 tryptone soya agar (TSA) or R2A agar at 28°C (Table 5). Subsequently, single
847 colonies were selected and grown overnight at 28°C while shaking at 130 rpm in
848 low-salt Luria broth (LB) (NaCl, 0.5 g/L; Tryptone, 10 g/L; Yeast Extract, 5 g/L).

849 Overnight cultures were resuspended to OD_{600}=0.05 in low-salt LB and 100 µL
850 were supplemented with 100 µL of purified effector proteins or culture filtrates to
851 a final OD_{600}=0.025 in clear 96 well flat-bottom polystyrene tissue culture plates
852 (Greiner CELLSTAR®, Sigma, Burlington, U.S.A). Culture plates were incubated in
853 a CLARIOstar plate reader (BMG LABTECH, Ortenberg, Germany) at 25°C with
854 double orbital shaking every 15 minutes and OD_{600} was measured every 15
855 minutes.

856 Filamentous fungal isolates were grown on PDA at 22°C, while for yeasts,
857 single colonies were selected and grown overnight in 5% PDB at 28°C while
858 shaking at 200 rpm. For yeasts overnight cultures were resuspended to
859 OD_{600}=0.01 in fresh 5% PDB supplemented with water, 10 µM FUN_011519 or 6
860 µM FUN_004580. For filamentous fungi, spores were harvested from PDA and
861 suspended in 5% PDB supplemented with 10 µM FUN_011519, 6 µM
862 FUN_004580 or water to a final concentration of 10^4 spores/mL. Next, 200 µL of
863 the fungal suspensions was aliquoted in clear 96-well flat bottom polystyrene
864 tissue-culture plates (Greiner CELLSTAR®, Sigma, Burlington, U.S.A). Plates were
865 incubated at 28°C, and fungal growth was imaged using an SZX10 stereo
866 microscope (Olympus, Tokyo, Japan) with EP50 camera (Olympus, Tokyo,
867 Japan).

868

869 **Microbial confrontation assays**

870 *R. necatrix* was grown on PDA for 14 days and mycelium disks of 5 mm diameter
871 were taken using a biopsy puncher (Kai Europe, Solingen, Germany). Single *R.*
872 *necatrix* disks were placed in the center of a PDA plate and 100 µL (OD_{600}=0.05)
873 of bacterial culture (Table 5), grown overnight in LB medium at 28°C at 130 rpm,

874 was added in proximity of the fungal disk with a spreader (n=5). After seven
875 days, pictures were taken. Experiment was repeated three times.
876
877 **Biocontrol assay**
878 *Bacillus drentensis, Sphingobium mellinum, Cellulosimicrobium cellulans* and
879 *Pseudoxanthomonas suwonensis* were grown overnight at 28°C in low-salt LB
880 while shaking at 130 rpm. Subsequently, the bacterial suspension was pelleted,
881 washed, and resuspended to OD_{600}=0.05 in water. Seeds of cotton cv. XLZ were
882 surface-sterilized with 2% sodium hypochlorite for ten minutes, washed three
883 times with sterile water, and then soaked for ten minutes the bacterial
884 suspension. Next, the seeds were transferred to sterile Petri dishes containing
885 filter paper moistened with each of the bacterial suspension and incubated in
886 darkness at room temperature. Once the seeds germinated, germlings were
887 transferred to potting soil in the greenhouse (16 hours light at 24°C and 8 hours
888 darkness at 22°C). Seven days after transfer to potting soil, the seedlings were
889 inoculated with mycelium of a 14-day-old *R. necatrix* culture in PDB. To this end,
890 the mycelium was pelleted, washed, and resuspended in 250 mL water. This
891 mycelial suspension was subsequently used for root-dip inoculation of the cotton
892 seedlings for 10 min, after which they were re-planted and 10 mL of mycelium
893 suspension was poured onto the pot in close proximity to the stem. At 14 days
894 post inoculation (dpi) disease symptoms were recorded. Experiment was
895 repeated three times.
896
897 **Data availability**
898 Genomes and genome annotation data have been submitted to NCBI under
899 BioProject PRJNA727191.

900

901 **Supporting information**

902 **Supplemental Table 1. Annotation of predicted effector proteins of *R.***
903 ***necatrix* strain R18.**

904 **Supplemental Table 2. Single nucleotide polymorphism ratios (SNPs in**
905 **%) and presence-absence variation for predicted effector genes in the *R.***
906 ***necatrix* strains sequenced in this study using *R. necatrix* strain R18 as a**
907 **reference.**

908 **Supplemental Table 3. Annotated secondary metabolite clusters of *R.***
909 ***necatrix* strain R18.**

910 **Supplemental Table 4. Bacterial strains used in this study.**

911 **Supplemental Table 5. Primers used in this study.**

912 **Supplemental Table 6. FUN_004580 homologs.**

913 **Supplemental Table 67. FUN_011519 homologs.**

914

915 **Acknowledgements**

916 EACC and DET acknowledge receipt of PhD fellowships from CONACyT, Mexico.
917 ALM is holder of a postdoctoral research fellow funded by the 'Fundación Ramón
918 Areces'. BPHJT acknowledges funding by the Alexander von Humboldt Foundation
919 in the framework of an Alexander von Humboldt Professorship endowed by the
920 German Federal Ministry of Education and Research, and is furthermore
921 supported by the Deutsche Forschungsgemeinschaft (DFG, German Research
922 Foundation) under Germany´s Excellence Strategy – EXC 2048/1 – Project ID:
923 390686111. The authors declare no conflict of interest exists.

924

925 **Author contributions**

Conceptualization: Edgar Chavarro-Carrero, Nick Snelders, Michael Seidl, Bart Thomma.

Formal analysis: Edgar Chavarro-Carrero, Nick Snelders, David Torres, Anton Kraege.

Investigation: Edgar Chavarro-Carrero, Nick Snelders, David Torres, Anton Kraege.

Resources: Ana López-Moral, Gabriella Petti, Wilko Punt, Jan Wieneke, Rómulo García-Velasco, Carlos López-Herrera.

Supervision: Nick Snelders, Michael Seidl, Bart Thomma.

Writing – Original Draft Preparation: Edgar Chavarro-Carrero, Nick Snelders, David Torres, Anton Kraege.

Writing – Review & Editing: Michael Seidl, Bart Thomma.

938 **REFERENCES**

939 Almagro, J. J. A., Tsirigos, K. D., Sønderby, C. K., Petersen, T. N., Winther, O.,
940 Brunak, S., von Heijne, G., and Nielsen, H. (2019). SignalP 5.0 improves
941 signal peptide predictions using deep neural networks. Nature
942 Biotechnology, 37: 420-423.

943 Badri, D. V., and Vivanco, J. M. (2009). Regulation and function of root exudates.
944 Plant Cell and Environment, 32: 666-681.

945 Bailly-Bechet, M., Haudry, A., and Lerat, E. (2014). "One code to find them all":
946 a perl tool to conveniently parse RepeatMasker output files. Mobile DNA, 5:
947 1-15.

948 Beilsmith, K., Thoen, M. P. M., Brachi, B., Gloss, A. D., Khan, M. H., and
949 Bergelson, J. (2019). Genome-wide association studies on the
950 phyllosphere microbiome: Embracing complexity in host–microbe
951 interactions. The Plant Journal, 97: 164-181.

952 Berendsen, R. L., Pieterse, C. M. J., and Bakker, P. A. H. M. (2012). The
953 rhizosphere microbiome and plant health. Trends in Plant Science, 17:
954 478-486.

955 Bertels, F., Silander, O. K., Pachkov, M., Rainey, P. B., and van Nimwegen, E.
956 (2014). Automated reconstruction of whole-genome phylogenies from
957 short-sequence reads. Molecular Biology and Evolution, 31: 1077-1088.

958 Blin, K., Shaw, S., Steinke, K., Villebro, R., Ziemert, N., Lee, S. Y., Medema, M.
959 H., and Weber, T. (2019). AntiSMASH 5.0: updates to the secondary
960 metabolite genome mining pipeline. Nucleic Acids Research, 47: 81–87.

961 Bormann, C., Baier, D., Hörr, I., Raps, C., Berger, J., Jung, G., and Schwarz, H.
962 (1999). Characterization of a novel, antifungal, chitin-binding protein from

963 *Streptomyces tendae* Tu□901 that interferes with growth polarity. Journal
964 of Bacteriology, 181: 7421-7429.
965 Bray, N. L., Pimentel, H., Melsted, P., and Pachter, L. (2016). Near-optimal
966 probabilistic RNA-seq quantification. Nature Biotechnology, 34: 525-527.
967 Bressan, M., Roncato, M., Bellvert, F., Comte, G., Haichar, F., Achouak, W., and
968 Berge, O. (2009). Exogenous glucosinolate produced by *Arabidopsis*
969 *thaliana* has an impact on microbes in the rhizosphere and plant roots.
970 Multidisciplinary Journal of Microbial Ecology, 3: 1243–1257.
971 Broekaert, W. F., Marien, W., Terras, F. R. G., De Bolle, M. F. C., Proost, P., Van
972 Damme, J., Dillen, L., Claeys, M., Rees, A. B., Vanderleyden, J., and
973 Cammue, B. P. A. (1992). Antimicrobial peptides from *Amaranthus*
974 *caudatus* seeds with sequence homology to the cysteine/glycine-rich
975 domain of chitin-binding proteins. Biochemistry, 31: 4308-4314.
976 Burton, J. N., Adey, A., Patwardhan, R. P., Qiu, R., Kitzman, J. O., and Shendure,
977 J. (2013). Chromosome-scale scaffolding of *de novo* genome assemblies
978 based on chromatin interactions. Nature Biotechnology, 31: 1119–1125.
979 Campos-Olivas, R., Hörr, I., Bormann, C., Jung, G., and Gronenborn, A. M.
980 (2001). Solution structure, backbone dynamics and chitin binding of the
981 anti-fungal protein from Streptomyces tendae TÜ901. Journal of Molecular
982 Biology, 308: 765-782.
983 Carresi, L., Pantera, B., Zoppi, C., Cappugi, G., Oliveira, A. L., Pertinhez, T. A.,
984 Spisni, A., Scala, A., and Pazzagli, L. (2006). Cerato-platanin, a phytotoxic
985 protein from *Ceratocystis fimbriata*: expression in *Pichia pastoris*,
986 purification and characterization. Protein Expression and Purification, 49:
987 159-167.

988 Cazorla, F. M., Duckett, S. B., Bergström, E. T., Noreen, S., Odijk, R.,
989 Lugtenberg, B. J. J., Thomas-Oates, J. E., and Bloemberg, G. V. (2006).
990 Biocontrol of avocado dematophora root rot by antagonistic *Pseudomonas*
991 *fluorescens* PCL1606 correlates with the production of 2-hexyl 5-propyl
992 resorcinol. Molecular Plant-Microbe Interactions, 19: 418–428.
993 Chai, Y. N., and Schachtman, D. P. (2022). Root exudates impact plant
994 performance under abiotic stress. Trends in Plant Science, 27: 80-91.
995 Chavarro-Carrero, E. A., Vermeulen, J. P., E. Torres, D., Usami, T., Schouten, H.
996 J., Bai, Y., Seidl, M. F., and Thomma, B. P. H. J. (2021). Comparative
997 genomics reveals the in planta-secreted *Verticillium dahliae* Av2 effector
998 protein recognized in tomato plants that carry the *V2* resistance locus.
999 Environmental Microbiology, 23: 1941–1958.
1000 Cook, D., Donzelli, B. G. G., Creamer, R., Baucom, D. L., Gardner, D. R., Pan, J.,
1001 Moore, N., Krasnoff, S. B., Jaromczyk, J. W., and Schardl, C. L. (2017).
1002 Swainsonine biosynthesis genes in diverse symbiotic and pathogenic fungi.
1003 Genes, Genomes, Genetics, 7: 1791-1797.
1004 Cordovez, V., Rotoni, C., Dini-Andreote, F., Oyserman, B., Carrión, V. J., and
1005 Raaijmakers, J. M. (2021). Successive plant growth amplifies genotype-
1006 specific assembly of the tomato rhizosphere microbiome. Science of the
1007 Total Environment, 772: 144825.
1008 Danecek, P., Bonfield, J. K., Liddle, J., Marshall, J., Ohan, V., Pollard, M. O.,
1009 Whitwham, A., Keane, T., McCarthy, S. A., Davies, R. M., and Li, H.
1010 (2021). Twelve years of SAMtools and BCFtools. Gigascience, 10: 1-4.
1011 Davey, J. W., Davis, S. J., Mottram, J. C., and Ashton, P. D. (2020). Tapestry:
1012 validate and edit small eukaryotic genome assemblies with long reads.
1013 BioRxiv, 2019–2020.

1014 de Guillen, K., Ortiz-Vallejo, D., Gracy, J., Fournier, E., Kroj, T., and Padilla, A.
1015 (2015). Structure analysis uncovers a highly diverse but structurally
1016 conserved effector family in phytopathogenic fungi. PLoS Pathogens, 11:
1017 1-27.
1018 de Jonge, R., and Thomma, B. P. H. J. (2009). Fungal LysM effectors:
1019 extinguishers of host immunity? Trends in Microbiology, 17: 151–157.
1020 de Jonge, R., van Esse, H. P., Kombrink, A., Shinya, T., Desaki, Y., Bours, R.,
1021 van der Krol, S., Shibuya, N., Joosten, M. H. A. J., and Thomma, B. P. H.
1022 J. (2010). Conserved fungal LysM effector Ecp6 prevents chitin-triggered
1023 immunity in plants. Science, 329: 953-955.
1024 Djamei, A., Schipper, K., Rabe, F., Ghosh, A., Vincon, V., Kahnt, J., Osorio, S.,
1025 Toghe, T., Fernie, A. R., Feussner, K., Meinicke, P., Stierhof; Y., Schwarz,
1026 H., Macek, B., Mann, M., and Kahmann, R. (2011). Metabolic priming by a
1027 secreted fungal effector. Nature, 478: 395-398.
1028 Dong, S., Raffaele, S., and Kamoun, S. (2015). The two-speed genomes of
1029 filamentous pathogens: waltz with plants. Current Opinion in Genetics and
1030 Development, 35: 57-65.
1031 Dudchenko, O., Batra, S. S., Omer, A. D., Nyquist, S. K., Hoeger, M., Durand, N.
1032 C., Shamin, M. S., Machol, I., Lander, E. S., Aiden, A. P., and Aiden, E. L.
1033 (2017). *De novo* assembly of the *Aedes aegypti* genome using Hi-C yields
1034 chromosome-length scaffolds. Science, 356: 92–95.
1035 Dudchenko, O., Shamim, M. S., Batra, S. S., Durand, N. C., Musial, N. T.,
1036 Mostofa, R., Pham, M., St Hilaire, B. G., Yao, W., Stamenova, E., Hoeger,
1037 M., Nyquist, S., Korchina, V., Pletch, K., Flanagan, J. P., Tomaszewicz, A.,
1038 McAloose, D., Perez-Estrada, C., Novak, B. J., Omer, R. D., and Aiden, E.
1039 L. (2018). The juicebox assembly tools module facilitates *de novo*

1040 assembly of mammalian genomes with chromosome-length scaffolds for
1041 under $1000. BioRxiv, 254797.
1042 Duplessis, S., Cuomo, C. A., Lin, Y., Aerts, A., Tisserant, E., Veneault-Fourrey,
1043 C., Joly, D., Hacquard, S., Amselem, J., Cantarel, B. L. Chiu, R., Coutinho,
1044 P. M., Feau, N., Field, M., Frey, P., Gelhaye, E., Goldberg, J., Grabherr, M.
1045 G., Kodira, C. D., Kohler, A., Kües, U., Lindquist, E. A., Lucas, S. M., Mago,
1046 R., Mauceli, E., Morin, E., Murat, C., Pangilinan, J. L., Park, R., Pearson,
1047 M., Quesneville, H., Rouhier, N., Sakthikumar, S., Salamov, A., Schmutz,
1048 J., Selles, B., Shapiro, H., Tanguay, P., Tuskan, G. A., Henrissat, B., van
1049 de Peer, Y., Rouzé, P., Ellis, J. G., Dodds, P. N., Schein, J. E., Zhong, S.,
1050 Hamelin, R. C., Grigoriev, I. V., Szabo, L. J., and Martin, F. (2011).
1051 Obligate biotrophy features unraveled by the genomic analysis of rust
1052 fungi. Proceedings of the National Academy of Sciences, 108: 9166-9171.
1053 Durand, N. C., Shamim, M. S., Machol, I., Rao, S. S. P., Huntley, M. H., Lander,
1054 E. S., and Aiden, E. L. (2016). Juicer provides a one-click system for
1055 analyzing loop-resolution Hi-C experiments. Cell Systems, 3: 95–98.
1056 Eguchi, N., Kondo, K. I., and Yamagishi, N. (2009). Bait twig method for soil
1057 detection of *Rosellinia necatrix*, causal agent of white root rot of Japanese
1058 pear and apple, at an early stage of tree infection. Journal of General Plant
1059 Pathology, 75: 325–330.
1060 Faino, L., Seidl, M. F., Shi-Kunne, X., Pauper, M., van den Berg, G. C.,
1061 Wittenberg, A. H., and Thomma, B. P. H. J. (2016). Transposons passively
1062 and actively contribute to evolution of the two-speed genome of a fungal
1063 pathogen. Genome Research, 26: 1091–1100.
1064 Fouché, S., Badet, T., Oggenfuss, U., Plissonneau, C., Francisco, C. S., and Croll,
1065 D. (2020). Stress-driven transposable element de-repression dynamics

1066 and virulence evolution in a fungal pathogen. Molecular Biology and
1067 Evolution, 37: 221-239.
1068 Frantzeskakis, L., Di Pietro, A., Rep, M., Schirawski, J., Wu, C., and Panstruga,
1069 R. (2020). Rapid evolution in plant–microbe interactions – a molecular
1070 genomics perspective. New Phytologist, 225: 1134-1142.
1071 Frantzeskakis, L., Kracher, B., Kusch, S., Yoshikawa-Maekawa, M., Bauer, S.,
1072 Pedersen, C., Spanu, P. D., Maekawa, T., Schulze-Lefert, P., and
1073 Panstruga, R. (2018). Signatures of host specialization and a recent
1074 transposable element burst in the dynamic one-speed genome of the
1075 fungal barley powdery mildew pathogen. BMC Genomics, 19: 381.
1076 Freitas, D. A., Leclerc, S., Miyoshi, A., Oliveira, S. C., Sommer, P. S. M.,
1077 Rodrigues, L., Correa-Junior, A., Gautier, M., Langella, P., Azevedo, V. A.,
1078 and Le Loir, Y. (2005). Secretion of *Streptomyces tendae* antifungal
1079 protein 1 by *Lactococcus lactis*. Brazilian Journal of Medical and Biological
1080 Research, 38: 1585-1592.
1081 Gan, P., Ikeda, K., Irieda, H., Narusaka, M., O'Connell, R. J., Narusaka, Y.,
1082 Takano, Y., Kubo, Y., and Shirasu, K. (2013). Comparative genomic and
1083 transcriptomic analyses reveal the hemibiotrophic stage shift of
1084 *Colletotrichum* fungi. New Phytologist, 197: 1236-1249.
1085 García-velasco, R., González-díaz, J. G., Domínguez-arizmendi, G., Ayala-
1086 escobar, V., and Aguilar-medel, S. (2012). *Rosellinia necatrix* in *Rosa* sp.,
1087 and an evaluation of its sensitivity to fungicides. Revista Chapingo, Serie
1088 Horticultura, 18: 39–54.
1089 Gel, B., Díez-Villanueva, A., Serra, E., Buschbeck, M., Peinado, M. A., and
1090 Malinverni, R. (2016). regioneR: an R/Bioconductor package for the

1091 association analysis of genomic regions based on permutation tests.
1092 Bioinformatics, 32: 289–291.
1093 Guillaumin, J., Mercier, S., and Dubos, B. (1982). Les pourridiés à Armillariella et
1094 Rosellinia en France sur vigne, arbres fruitiers et cultures florales I.
1095 Etiologie et symptomatologie. Agronomie, 2: 71–80.
1096 Ingham, A. B., and Moore, R. J. (2007). Recombinant production of antimicrobial
1097 peptides in heterologous microbial systems. Biotechnology and Applied
1098 Biochemistry, 47: 1-9.
1099 Ismail, I. A., and Able, A. (2016). Secretome analysis of virulent *Pyrenophora*
1100 *teres* f. *teres* isolates. Proteomics, 16: 2625-2636.
1101 Jeffares, D. C., Jolly, C., Hoti, M., Speed, D., Shaw, L., Rallis, C., Balloux, F.,
1102 Dessimoz, C., Bähler, J., and Sedlazeck, F. J. (2017). Transient structural
1103 variations have strong effects on quantitative traits and reproductive
1104 isolation in fission yeast. Nature Communications, 8: 1-11.
1105 Jumper, J., Evans, R., Pritzel, A., Green, T., Figurnov, M., Ronneberger, O.,
1106 Tunyasuvunakool, K., Bates, R., Žídek, A., Potapenko, A., Bridgland, A.,
1107 Meyer, C., Kohl, S. A. A., Ballard, A. J., Cowie, A., Romera-Paredes, B.,
1108 Nikolov, S., Jain, R., Adler, J., Back, T., Petersen, S., Reiman, D., Clancy,
1109 E., Zielinski, M., Steinegger, M., Pacholska, M., Berghammer, T.,
1110 Bodenstein, S., Silver, D., Vinyals, O., Senior, A. W., Kavukcuoglu, K.,
1111 Kohli, P., and Hassabis, D. (2021). Highly accurate protein structure
1112 prediction with AlphaFold. Nature, 596: 583–589.
1113 Katoh, K., and Standley, D. M. (2013). MAFFT multiple sequence alignment
1114 software version 7: Improvements in performance and usability. Molecular
1115 Biology and Evolution, 30: 772–780.

1116 Kawaide, H. (2006). Biochemical and molecular analyses of gibberellin
1117 biosynthesis in fungi. Bioscience, Biotechnology, and Biochemistry, 70:
1118 583-590.
1119 Kelley, L. A., Mezulis, S., Yates, C. M., Wass, M. N., and Sternberg, M. J. E.
1120 (2015). The Phyre2 web portal for protein modeling, prediction and
1121 analysis. Nature Protocols, 10: 845-858.
1122 Kombrink, A., and Thomma, B. P. H. J. (2013). LysM effectors: secreted proteins
1123 supporting fungal life. PLoS Pathogens, 9: 1–4.
1124 Koren, S., Walenz, B. P., Berlin, K., Miller, J. R., Bergman, N. H., and Phillippy,
1125 A. M. (2017). Canu: scalable and accurate long-read assembly via
1126 adaptive k-mer weighting and repeat separation. Genome Research, 27:
1127 722–736.
1128 Langmead, B., and Salzberg, S. L. (2012). Fast gapped-read alignment with
1129 Bowtie 2. Nature Methods, 9: 357–359.
1130 Lenarčič, T., Albert, I., Böhm, H., Hodnik, V., Pirc, K., Zavec, A. B., Podobnik, M.,
1131 Pahovnik, D., Žagar, E., Pruitt, R., Greimel, P., Yamaji-Hasegawa, A.,
1132 Kobayashi, T., Zienkiewicz, A., Gömann, J., Mortimer, J. C., Fang, L.,
1133 Mamode-Cassim, A., Deleu, M., Lins, L., Oecking, C., Feussner, I.
1134 Mongrand, S., Anderluh, G., and Nürnberger, T. (2017). Eudicot plant-
1135 specific sphingolipids determine host selectivity of microbial NLP
1136 cytolysins. Science, 358: 1431-1434.
1137 Lo Presti, L., Lanver, D., Schweizer, G., Tanaka, S., Liang, L., Tollot, M., Zuccaro,
1138 A., Reissmann, S., and Kahmann, R. (2015). Fungal effectors and plant
1139 susceptibility. The Annual Review of Plant Biology, 66: 513-545.
1140 Lu, Y., Xue, Q., Eisele, M. R., Sulistijo, E. S., Brower, K., Han, L., Amir, E. D.,
1141 Pe'er, D., Miller-Jensen, K., and Fan, R. (2015). Highly multiplexed

1142 profiling of single-cell effector functions reveals deep functional
1143 heterogeneity in response to pathogenic ligands. Proceedings of the
1144 National Academy of Sciences, 112: E607-E615.
1145 Luciano-Rosario, D., Eagan, J. L., Aryal, N., Dominguez, E. G., Hull, C. M., and
1146 Keller, N. P. (2022). The hydrophobin gene family confers a fitness trade-
1147 off between spore dispersal and host colonization in *Penicillium expansum*.
1148 mBio, e02754-22.
1149 Malinovsky, F. G., Fangel, J. U., and Willats, W. G. T. (2014). The role of the cell
1150 wall in plant immunity. Frontiers in Plant Science, 5: 1-12.
1151 Martins, J. C., Maes, D., Loris, R., Pepermans, H. A. M., Wyns, L., Willen, R., and
1152 Verheyden, P. (1996). ^{1}H NMR study of the solution structure of Ac-AMP2,
1153 a sugar binding antimicrobial protein isolated from *Amaranthus caudatus*.
1154 Journal of Molecular Biology, 258: 322-333.
1155 Oggenfuss, U., Badet, T., Wicker, T., Hartmann, F. E., Singh, N. K., Abraham, L.,
1156 Karisto, P., Vonlanthen, T., Mundt, C., McDonald, B. A., and Croll, D.
1157 (2021). A population-level invasion by transposable elements triggers
1158 genome expansion in a fungal pathogen. eLife, 10: e69249.
1159 Ou, S., Su, W., Liao, Y., Chougule, K., Agda, J. R. A., Hellinga, A. J., Blanco-
1160 Lugo, C. S., Elliot, T. A., Waren, D., Peterson, T., Jiang, N., Hirsch, C. N.,
1161 and Hufford, M. B. (2019). Benchmarking transposable element annotation
1162 methods for creation of a streamlined, comprehensive pipeline. Genome
1163 Biology, 20: 275.
1164 Palmer, J., and Stajich, J. E. (2017). Funannotate: Eukaryotic genome
1165 annotation pipeline. Retrieved from
1166 https://funannotate.readthedocs.io/en/latest/

1167 Pérez-Jaramillo, J. E., Mendes, R., and Raaijmakers, J. M. (2016). Impact of
1168 plant domestication on rhizosphere microbiome assembly and functions.
1169 Plant Molecular Biology, 90: 635-644.
1170 Pérez-Jiménez, R. M., Jiménez-Díaz, R. M., and López-Herrera, C. J. (2002).
1171 Somatic incompatibility of *Rosellinia necatrix* on avocado plants in
1172 southern Spain. Mycological Research, 106: 239–244.
1173 Pliego, C., Kanematsu, S., Ruano-Rosa, D., de Vicente, A., López-Herrera, C.,
1174 Cazorla, F. M., and Ramos, C. (2009). GFP sheds light on the infection
1175 process of avocado roots by *Rosellinia necatrix*. Fungal Genetics and
1176 Biology, 46: 137–145.
1177 Quinlan, A. R., and Hall, I. M. (2010). BEDTools: a flexible suite of utilities for
1178 comparing genomic features. Bioinformatics, 26: 841-842.
1179 Rademacher, W., and Graebe, J. E. (1979). Gibberellin A4 produced by
1180 *Sphaceloma manihoticola*, the cause of the super elongation disease of
1181 cassava (*Manihot esculenta*). Biochemical and Biophysical Research
1182 Communications, 91: 35-40.
1183 Rafaelle, S., Farrer, R. A., Cano, L. M., Studholme, D. J., Maclean, D., Thines, M.,
1184 Jiang, R. H. Y., Zody, M. C., Kunjeti, S. G., Donofrio, N. M., Meyers, B. C.,
1185 Nusbaum, C., and Kamoun, S. (2010). Genome evolution following host
1186 jumps in the irish potato famine pathogen lineage. Science, 330: 1540-
1187 1543.
1188 Raffaele, S., and Kamoun, S. (2012). Genome evolution in filamentous plant
1189 pathogens: why bigger can be better. Nature Reviews Microbiology, 10:
1190 417-430.
1191 Rocafort, M., Bowen, J. K., Hassing, B., Cox, M. P., McGreal, B., de la Rosa, S.,
1192 Plummer, K. M., Bradshaw, R. E., and Mesarich, C. H. (2022). The

1193 *Venturia inaequalis* effector repertoire is dominated by expanded families
1194 with predicted structural similarity, but unrelated sequence, to avirulence
1195 proteins from other plant-pathogenic fungi. BMC Biology, 20: 1-24.
1196 Rovenich, H., Boshoven, J. C., and Thomma, B. P. H. J. (2014). Filamentous
1197 pathogen effector functions: of pathogens, hosts and microbiomes.
1198 Current Opinion in Plant Biology, 20: 96-103.
1199 Sadat, S. S., Khani, S., Goudarzi, M., Zare-Zardini, H., Shams-Ghahfarokhi, M.,
1200 Jamzivar, F., and Razzaghi-Abyaneh, M. (2021). Characterization,
1201 biological activity, and mechanism of action of a plant-based novel
1202 antifungal peptide, Cc-AFP1, isolated from *Carum carvi*. Frontiers in
1203 Cellular and Infection Microbiology, 11: 1-12.
1204 Santhanam, P., Van Esse, H.P., Albert, I., Faino, L., Nürnberger, T., and
1205 Thomma, B.P.H.J. (2013). Evidence for functional diversification within a
1206 fungal Nep1-like protein family. Molecular Plant Microbe Interactions, 26:
1207 278–286.
1208 Sawai, K., Okuno, T., Fujioka, H., and Furuya, M. (1983). The relation between
1209 the phytotoxicity of Cythochalasin E and its molecular structure. Annals of
1210 the Phytopathological Society of Japan, 49: 262-265.
1211 Schwessinger, B., Sperschneider, J., Cuddy, W. S., Garnica, D. P., Miller, M. E.,
1212 Taylor, J. M., Dodds, P. N., Figueroa, M., Park, R. F., and Rathjen, J. P.
1213 (2018). A near-complete haplotype-phased genome of the dikaryotic
1214 wheat stripe rust fungus *Puccinia striiformis* f. sp. *Tritici* reveals high
1215 interhaplotype diversity. mBio, 9: e02275-17.
1216 Seidl, M. F., and Thomma, B. P. H. J. (2014). Sex or no sex: evolutionary
1217 adaptation occurs regardless. Bioessays, 36: 335-345.

1218 Seidl, M. F., and Thomma, B. P. H. J. (2017). Transposable elements direct the
1219 coevolution between plants and microbes. Trends in Genetics, 33: 842–
1220 851.
1221 Seidl, M. F., and van den Ackerveken, G. (2019). Activity and phylogenetics of
1222 the broadly occurring family of microbial nep1-like proteins. Annual Review
1223 of Phytopathology, 57: 367–386.
1224 Seidl, M. F., Kramer, H. M., Cook, D. E., Fiorin, G. L., van den Berg, G. C. M.,
1225 Faino, L., and Thomma, B. P. H. J. (2020). Repetitive elements contribute
1226 to the diversity and evolution of centromeres in the fungal genus
1227 *verticillium*. MBio, 11: 1–22.
1228 Shi-Kunne, X., Faino, L., van den Berg G. C. M., Thomma B. P. H. J., and Seidl,
1229 M. F. (2018). Evolution within the fungal genus *Verticillium* is characterized
1230 by chromosomal rearrangement and gene loss. Environmental
1231 Microbiology, 20: 1362-1373.
1232 Shimizu, T., Kanematsu, S., and Yaegashi, H. (2018). Draft genome sequence
1233 and transcriptional analysis of *Rosellinia necatrix* infected with a virulent
1234 mycovirus. Phytopathology, 108: 1206–1211.
1235 Shimizu, T., Tsutae, I., and Kanematsu, S. (2014). Functional analysis of a
1236 melanin biosynthetic gene using RNAi-mediated gene silencing in *Rosellinia*
1237 *necatrix*. Fungal Biology, 118: 413-421.
1238 Simão, F. A., Waterhouse, R. M., Ioannidis, P., Kriventseva, E. V., and Zdobnov,
1239 E. M. (2015). BUSCO: Assessing genome assembly and annotation
1240 completeness with single-copy orthologs. Bioinformatics, 31: 3210–3212.
1241 Sivanesan, A., and Holliday, P. (1972). *Rosellinia necatrix*. In Description of
1242 Pathogenic Fungi and Bacteria, (p. 352).

1243 Smercina, D. N., Bailey, V. L., and Hofmockel, K. S. (2021). Micro on a
1244 macroscale: relating microbial-scale soil processes to global ecosystem
1245 function. FEMS Microbiology Ecology, 97: 1-11.
1246 Snelders, N. C., Boshoven, J. C., Song, Y., Schmitz, N., Fiorin, G. L., Rovenich,
1247 H., van den Berg, G. C. M., Torres, D. E., Petti, G. C., Prockl, Z., Faino, L.,
1248 Seidl, M. F., and Thomma, B. P. H. J. (2023). A highly polymorphic effector
1249 protein promotes fungal virulence through suppression of plant-associated
1250 Actinobacteria. New Phytologist, doi:10.1111/nph.18576
1251 Snelders, N. C., Kettles, G. J., Rudd, J. J., and Thomma, B. P. H. J. (2018). Plant
1252 pathogen effector proteins as manipulators of host microbiomes? Molecular
1253 Plant Pathology, 19: 257-259.
1254 Snelders, N. C., Petti, G. C., van den Berg, G. C. M., Seidl, M. F., and Thomma,
1255 B. P. H. J. (2021). An ancient antimicrobial protein co-opted by a fungal
1256 plant pathogen for *in planta* mycobiome manipulation. Proceedings of the
1257 National Academy of Sciences, 118: e2110968118.
1258 Snelders, N. C., Rovenich, H., and Thomma, B. P. H. J. (2022). Microbiota
1259 manipulation through the secretion of effector proteins is fundamental to
1260 the wealth of lifestyles in the fungal kingdom. FEMS Microbiology Reviews,
1261 46: 1-16.
1262 Snelders, N. C., Rovenich, H., Petti, G. C., Rocafort, M., van den Berg, G. C. M.,
1263 Vorholt, J. A., Mesters, J. R., Seidl, M., Nijland, R., and Thomma, B. P. H.
1264 J. (2020). Microbiome manipulation by a soil-borne fungal plant pathogen
1265 using effector proteins. Nature Plants, 6: 1365-1374.
1266 Spanu, P. D. (2017). Cereal immunity against powdery mildews targets RNase-
1267 Like Proteins associated with Haustoria (RALPH) effectors evolved from a
1268 common ancestral gene. New Phytologist, 213: 1301-1314.

1269 Sperschneider, J., Dodds, P. N., Gardiner, D. M., Singh, K. B., and Taylor, J. M.
1270 (2018). Improved prediction of fungal effector proteins from secretomes
1271 with EffectorP 2.0. Molecular Plant Pathology, 19: 2094-2110.
1272 Stam, R., Münsterkötter, M., Pophaly, S. D., Fokkens, L., Sghyer, H., Güldener,
1273 U., Hückelhoven, R., and Hess, M. (2018). A new reference genome shows
1274 the one-speed genome structure of the barley pathogen *Ramularia collo-*
1275 *cygni*. Genome Biology and Evolution, 10: 3243–3249.
1276 Stamatakis, A. (2014). RAxML version 8: A tool for phylogenetic analysis and
1277 post-analysis of large phylogenies. Bioinformatics, 30: 1312–1313.
1278 Stancu, M. C., Van Roosmalen, M. J., Renkens, I., Nieboer, M. M., Middelkamp,
1279 S., de Ligt, J., Pregno, G., Giachino, D., Mandrile, G., Espejo, J. V.,
1280 Korzelius, J., de Bruijn, E., Cuppen, E., Talkowski, M. E., Marschall, T., de
1281 Ridder, J., and Kloosterman, W. P. (2017). Mapping and phasing of
1282 structural variation in patient genomes using nanopore sequencing. Nature
1283 Communications, 8: 1–13.
1284 Stergiopoulos, I., Collemare, J., Mehrabi, R., and de Wit, P. J. G. M. (2013).
1285 Phytotoxic secondary metabolites and peptides produced by plant
1286 pathogenic *Dothideomycete* fungi. FEMS Microbiology Review, 37: 67-93.
1287 Sztejnberg, A., and Madar, Z. (1980). Host range of *Dematophora necatrix*, the
1288 cause of white root rot disease in fruit trees. Plant Disease, 64: 662–664.
1289 Takai, S. (1974). Pathogenicity and cerato-ulmin production in *Ceratocystis ulmi*.
1290 Nature, 252: 124-126.
1291 Talbot, N. J., Kershaw, M. J., Wakley, G. E., de Vries, O. M. H., Wessels, J. G. H.,
1292 and Hamer, J. E. (1996). *MPG1* encodes a fungal hydrophobin involved in
1293 surface interaction during infection-related development of *Magnaporthe*
1294 *grisea*. The Plant Cell, 8: 985-999.

1295 Thomas, D. D. (1978). Cytochalasin effects in plants and eukaryotic microbial
1296 systems. Frontiers in Biology, 46: 257-275.
1297 Thomma, B. P. H. J., Seidl, M. F., Shi-Kunne, X., Cook, D. E., Bolton, M. D., van
1298 Kan, J. A. L., and Faino, L. (2016). Mind the gap; seven reasons to close
1299 fragmented genome assemblies. Fungal Genetics and Biology, 90: 24–30.
1300 Tian, H., Fiorin, G. L., Kombrink, A., Mesters, J. R., and Thomma, B. P. H. J.
1301 (2022). Fungal dual-domain LysM effectors undergo chitin-induced
1302 intermolecular, and not intramolecular, dimerization. Plant Physiology,
1303 190: 2033-2044.
1304 Tian, H., MacKenzie, C. I., Rodriguez-Moreno, L., van den Berg, G. C. M., Chen,
1305 H., Rudd, J. J., Mesters, J. R., and Thomma, B. P. H. J. (2021). Three LysM
1306 effectors of Zymoseptoria tritici collectively disarm chitin-triggered plant
1307 immunity. Molecular Plant Pathology, 22: 683-693.
1308 Törönen, P., and Holm, L. (2022). PANNZER-A practical tool for protein function
1309 prediction. Protein Science, 31: 118-128.
1310 Torres, D. E., Oggenfuss, U., Croll, D., and Seidl, M. (2020). Genome evolution
1311 in fungal plant pathogens: looking beyond the two-speed genome model.
1312 Fungal Biology Reviews, 34: 136-143.
1313 Underwood, W. (2012). The plant cell wall: a dynamic barrier against pathogen
1314 invasion. Frontiers in Plant Science, 3: 1-6.
1315 Varoquaux, N., Liachko, I., Ay, F., Burton, J. N., Shendure, J., Dunham, M. J.,
1316 Vert, J. P., and Noble, W. S. (2015). Accurate identification of centromere
1317 locations in yeast genomes using Hi-C. Nucleic Acids Research, 43: 5331–
1318 5339.
1319 Virtanen, P., Gommers, R., Oliphant, T. E., Haberland, M., Reddy, T.,
1320 Cournapeau, D., Burovski, E., Peterson, P., Weckesser, W., Bright, J., van

1321 der Walt, S. J., Brett, M., Wilson, J., Millman, K. J., Mayorov, N., Nelson, A.
1322 R. J., Jones, E., Kern, R., Larson, E., Carey, C. J., Polat, İ., Feng, Y.,
1323 Moore, E. W., VanderPlas, J., Laxalde, D., Perktold, J., Cimrman, R.,
1324 Henriksen, I., Quintero, E. A., Harris, C. R., Archibald, A. M., Ribeiro, A.,
1325 Pedregosa, F., van Mulbregt, P., and SciPy 1.0 Contributors. (2020). SciPy
1326 1.0: fundamental algorithms for scientific computing in Python. Nature
1327 Methods, 17: 261–272.
1328 Walton, J. D. (1990). Peptide phytotoxins from plant pathogenic fungi. In
1329 Biochemistry of peptide antibiotics. Kleinkauf, H., and von Dohren, H.
1330 (eds). Berlin, 179-203 pp.
1331 Wang, E., Schornack, S., Marsh, J. F., Gobbato, E., Schwessinger, B., Eastmond,
1332 P., Schultze, M., Kamoun, S., and Oldroyd, G. E. D. (2012). A common
1333 signaling process that promotes Mycorrhizal and Oomycete colonization of
1334 plants. Current Biology, 22: 2242-2246.
1335 Wang, J. R., Holt, J., McMillan, L., and Jones, C. D. (2018). FMLRC: Hybrid long
1336 read error correction using an FM-index. BMC Bioinformatics, 19: 1–11.
1337 Wawra, S., Fesel, P., Widmer, H., Neumann, U., Lahrmann, U., Becker, S.,
1338 Hehemann, J., Langen, G., and Zuccaro, A. (2019). FGB1 and WSC3 are *in*
1339 *planta*-induced *β*-glucan-binding fungal lectins with different functions.
1340 New Phytologist, 222: 1493-1506.
1341 Weiberg, A., Wang, M., Bellinger, M., and Jin, H. (2014). Small RNAs: a new
1342 paradigm in plant-microbe interactions. The Annual Review of
1343 Phytopathology, 52: 495-516.
1344 Weinert, N. Piceno, Y., Ding, G., Meincke, R., Heuer, H., Berg, G., Schloter, M.,
1345 Andersen, G., and Smalla, K. (2011). PhyloChip hybridization uncovered
1346 an enormous bacterial diversity in the rhizosphere of different potato

cultivars: many common and few cultivar-dependent taxa. FEMS Microbiology Ecology, 75: 497-506.

Wick, R. (2018). Porechop. Retrieved from https://github.com/rrwick/Porechop

Wilson, R. A., and McDowell, J. M. (2022). Recent advances in understanding of fungal and oomycete effectors. Current Opinion in Plant Biology, 68: 102228.

Wingfield, B. D., Berger, D. K., Coetzee, M. P. A., Duong, T. A., Martin, A., Pham, N. Q., van den Berg, N., Wilken, P. M., Arun Chinnappa, K. S., Barnes, I., Buthelezi, S., Dahanayaka, B. A., Durán, A., Engelbrecht, J., Feurtey, A., Fourie, A., Fourie, G., Hartley, J., Kabwe, E. N. K., Maphosa, M., Mensah, D. L. N., Nsibo, D. L., Potgieter, L., Poudel, B., Stukenbrock, E. H., Thomas, C., Vaghefi, N., Welgemoed, T., and Wingfield, M. J. (2022). IMA genome-F17: Draft genome sequences of an *Armillaria* species from Zimbabwe, *Ceratocystis colombiana*, *Elsinoë necatrix*, *Rosellinia necatrix*, two genomes of *Sclerotinia minor*, short-read genome assemblies and annotations of four *Pyrenophora teres* isolates from barley grass, and a long-read genome assembly of *Cercospora zeina.* IMA Fungus, 13: 1-22.

Xu, D., Xue, M., Shen, Z., Jia, X., Hou, X., Lai, D., and Zhou, L. (2021). Phytotoxic secondary metabolites from fungi. Toxins, 13: 1-65.

Zhalnina, K., Louie, K. B., Hao, Z., Mansoori, N., Nunes de Rocha, U., Shi, S., Cho, H., Karaoz, U., Loqué, D., Bowen. B. P., Firestone, M. K., Northen, T. R., and Brodie, E. L. (2018). Dynamic root exudate chemistry and microbial substrate preferences drive patterns in rhizosphere microbial community assembly. Nature Microbiology, 3: 470-480.

Zhang, Y., and Skolnick J. (2005). TM-align: a protein structure alignment algorithm based on the TM-score. Nucleid Acids Research, 33: 2302–2309.

1373 Zhao, Z., Ying, Y., Hung, Y., and Tang, Y. (2019). Genome mining reveals
1374 *Neurospora crassa* can produce the salicylaldehyde sordarial. Journal of
1375 Natural Products, 82: 1029-1033.